HHS Public Access

Author manuscript

Neuropharmacology. Author manuscript; available in PMC 2021 January 01.

Published in final edited form as:

Neuropharmacology. 2020 January 01; 162: 107837. doi:10.1016/j.neuropharm.2019.107837.

NEONATAL ETHANOL EXPOSURE TRIGGERS APOPTOSIS IN THE MURINE RETROSPLENIAL CORTEX: ROLE OF INHIBITION OF NMDA RECEPTOR-DRIVEN ACTION POTENTIAL FIRING

Clark W. Bird, **Megan J. Barber**, **Hilary R. Post**, **Belkis Jacquez**, **Glenna J. Chavez**, **Nicholas G. Faturos**[a], **C. Fernando Valenzuela**

Department of Neurosciences, School of Medicine, University of New Mexico Health Sciences Center Albuquerque, New Mexico, U.S.A.

Abstract

Exposure to ethanol during the last trimester equivalent of human pregnancy causes apoptotic neurodegeneration in the developing brain, an effect that is thought to be mediated, in part, by inhibition of NMDA receptors. However, NMDA receptors can rapidly adapt to the acute effects of ethanol and are ethanol resistant in some populations of developing neurons. Here, we characterized the effect of ethanol on NMDA and non-NMDA receptor-mediated synaptic transmission in the retrosplenial cortex (RSC), a brain region involved in the integration of different modalities of spatial information that is among the most sensitive regions to ethanol-induced neurodegeneration. A single four-hour exposure to ethanol vapor of 7-day-old transgenic mice that express the Venus fluorescent protein in interneurons triggered extensive apoptosis in the RSC. Slice electrophysiological recordings showed that bath-applied ethanol inhibits NMDA and non-NMDA receptor excitatory postsynaptic currents (EPSCs) in pyramidal neurons and interneurons; however, we found no evidence of acute tolerance development to this effect after the four-hour *in-vivo* ethanol vapor exposure. Acute bath application of ethanol reduced action potential firing evoked by synaptic stimulation to a greater extent in pyramidal neurons than interneurons. Submaximal inhibition of NMDA EPSCs, but not non-NMDA EPSCs, mimicked the acute effect of ethanol on synaptically-evoked action potential firing. These findings indicate that partial inhibition of NMDA receptors by ethanol has sizable effects on the excitability of glutamatergic and GABAergic neurons in the developing RSC, and suggest that positive allosteric modulators of these receptors could ameliorate ethanol intoxication-induced neurodegeneration during late stages of fetal development.

Corresponding Author: C. Fernando Valenzuela, MD, PhD, Department of Neurosciences, MSC08 4740, 1 University of New Mexico, Albuquerque, NM 87131-0001, Phone (505) 272-3128, Fax (505) 272-8082, fvalenzuela@salud.unm.edu.

[a]Present address: Kavli Institute,The Faculty of Medicine and Health Sciences, Norwegian University of Science and Technology, Postboks 8905, 7491 Trondheim, Norway

Keywords

fetal; alcohol; ethanol; development; cortex; retrosplenial; apoptosis; glutamate; electrophysiology; neonatal

1. Introduction

Alcohol consumption during pregnancy causes Fetal Alcohol Spectrum Disorders characterized by a wide range of physical, behavioral, and cognitive deficits (Hoyme et al., 2016). Exposure to ethanol during fetal development is a common cause of intellectual disability across the globe (Popova et al., 2017). Fetal ethanol exposure has lifelong consequences that vary from person to person depending on many factors, including the timing and pattern of gestational ethanol consumption.

Ethanol can affect multiple processes across the different stages of embryonic and fetal development. Studies have demonstrated that the last trimester of pregnancy is one of the periods where ethanol is consumed in human populations (Dukes et al., 2017; Ethen et al., 2009; Himes et al., 2015; Murphy et al., 2014), which is particularly concerning as this is a time period of major brain growth and early synaptic development (Cudd, 2005; Kostovic and Jovanov-Milosevic, 2006). In addition, ethanol is among the excipients contained in medications that are administered to very low birth weight neonates leading to significant exposure during a critical period of neuronal circuit refinement (Akinmboni et al., 2018). Sanitizers used before inserting hands into isolette incubators can also release enough alcohol vapor to produce significant exposure in premature babies (Hsieh et al., 2018). A large body of experimental evidence indicates that ethanol use during late pregnancy can have striking effects on child behavior, particularly when consumed in a binge-like manner (Niclasen et al., 2014).

Studies with rodent and non-human primate models of third trimester-equivalent ethanol exposure suggest that ethanol acts, in part, by causing apoptotic neurodegeneration (Creeley and Olney, 2013; Farber et al., 2010; Granato and Dering, 2018; Heaton et al., 2003; Nikolic et al., 2013; Saito et al., 2016). Importantly, a similar effect has been observed with other neuropharmacological agents; namely, volatile and intravenous anesthetics, benzodiazepines, barbiturates, and anticonvulsants (Olney, 2014). A decrease in excitability is the most likely trigger of the apoptotic response produced by these agents in the neocortex (Lebedeva et al., 2017; Lotfullina and Khazipov, 2018). Inhibition of network activity in the developing neocortex increases the number of apoptotic cells, whereas stimulation of neuronal activity has the opposite effect via activity-dependent release of brain-derived neurotrophic factor (BDNF) and stimulation of the phosphatidylinositol 3-kinase/Akt pathway (Golbs et al., 2011; Heck et al., 2008; Kirischuk et al., 2017). The finding that NMDA receptor antagonists (e.g., MK-801 and ketamine) partially mimic the inhibitory effects of ethanol on network activity, as well as its apoptotic actions suggests that inhibition of NMDA receptors plays a central role in the mechanism responsible for ethanol-induced neurodegeneration (Lebedeva et al., 2017; Lotfullina and Khazipov, 2018). The acute effect of ethanol on NMDA receptors depends on factors such as subunit composition,

phosphorylation state, and association with other proteins (Moykkynen and Korpi, 2012; Ron and Wang, 2009). In the rat CA3 hippocampus and layer II/III neocortex, slice electrophysiological experiments suggest that NMDA receptors can be relatively insensitive to acute ethanol exposure during the first week of life; in contrast, AMPA receptors are more sensitive in CA3 pyramidal neurons (Mameli et al., 2005; Sanderson et al., 2009). Importantly, NMDA receptors rapidly adapt to the continuous presence of ethanol in some neuronal populations (e.g. CA1 hippocampal pyramidal neurons); this acute tolerance to ethanol (defined as a reduced response to a single dose of ethanol during exposure (Kalant, 1993)) can develop within 15–30 minutes of exposure and can lead to rebound facilitation of NMDA currents after washout, an effect that could be mediated by alterations in the phosphorylation state of the GluN2B subunit (Ron and Wang, 2009; Wu et al., 2011). However, it is currently unknown if acute tolerance occurs in developing neurons that undergo ethanol-induced apoptosis and if it limits the contribution of NMDA receptor inhibition to alterations in neuronal excitability and survival. Moreover, it remains to be determined if ethanol has similar effects on NMDA receptor function in developing pyramidal neurons and interneurons.

In this study, we characterized the effect of ethanol on glutamatergic transmission in developing neurons of the retrosplenial cortex (RSC), a brain region that plays a central role in the integration of spatial information and is particularly sensitive to ethanol-induced neurodegeneration (Ikonomidou et al., 1999; Mitchell et al., 2018; Saito et al., 2007). We used a 4-h ethanol vapor inhalation paradigm to induce apoptotic neurodegeneration in the RSC. Using slice electrophysiological techniques, we measured the acute effect of bath-applied ethanol on NMDA and non-NMDA excitatory postsynaptic currents (EPSCs), not only in developing pyramidal neurons but also in interneurons, which are particularly susceptible to ethanol-induced apoptosis (Bird et al., 2018; Saito et al., 2019). To determine if ionotropic glutamate receptors develop acute tolerance to the effect of ethanol, these recordings were obtained from non-exposed control animals and animals exposed to ethanol for 4 h in a vapor chamber. Finally, we measured the effect of acute bath application of ethanol on action potential firing triggered by synaptic stimulation and the contribution of inhibition of glutamate ionotropic receptors to this effect.

2. Materials and methods

All animal procedures were approved by the Institutional Animal Care and Use Committee of the University of New Mexico Health Sciences Center and adhered to the U.S. Public Health Service policy on humane care and use of laboratory animals.

2.1. Animals

We used transgenic mice that express the fluorescent protein Venus in GABAergic and glycinergic interneurons (Venus-vesicular GABA transporter (VGAT) mice; generously provided by Dr. Yanagawa, Department of Genetic and Behavioral Neuroscience, Gunma University Graduate School of Medicine, Maebashi, Japan) (Wang et al., 2009). Mice were housed at 22 °C on a reverse 12-h light/dark cycle (lights on at 8 PM) with standard chow and water available *ad libitum.* Breeding of Venus-VGAT mice and genotyping were

performed as previously described (Bird et al., 2018). The average number of pups per litter was 8.2 ± 0.32 (n = 25). The number of Venus positive pups per litter was 4.4 ± 0.29 (n = 25). The average pup weight at postnatal day (P) 2 was 1.58 ± 0.05 g (n = 25). Male and female pups were used for the experiments.

2.2. Ethanol vapor chamber exposure

Pups and dams were exposed to either air or vaporized ethanol (95%, Koptec, King of Prussia, PA) for 4 h (approximately 10 am-2 pm) on P7. Ethanol vapor exposures took place in custom-built ethanol vapor chambers (Morton et al., 2014). Ethanol vapor concentrations measured with a breathalyzer (Intoximeters, St. Louis, MO) were 8–9 g/dl. To measure blood ethanol concentration (BECs) in pups, mice were anesthetized with isoflurane at different time points during and after vapor chamber exposure, decapitated, and trunk blood was collected using heparinized hematocrit tubes (Drummond Scientific, Broomall, PA). Heparinized blood (20 μl) was mixed with 0.5 N perchloric acid (380 μl) and then with 0.3 M potassium carbonate (400 μl). Samples were centrifuged at 13,000 rpm for 10 min at 4 °C. Supernatants were collected and stored in sealed tubes at −20 °C. Blood ethanol concentrations were measured using an alcohol dehydrogenase-based assay (Kelly and Lawrence, 2008).

2.3. Quantification of apoptotic cell death

Mice were deeply anesthetized with ketamine (250 mg/kg intraperitoneally) and transcardially perfused as previously described (Bird et al., 2018) before (control) or at various intervals after ethanol exposure (end of exposure and 2, 4, or 8 h post-exposure). Following perfusion with 4% paraformaldehyde (PFA, 4% w/v in phosphate buffered saline (PBS), pH 7.4), brains were incubated in 4% PFA for 48 h and then cryoprotectected in 30% sucrose (w/v in PBS) for 48 h. Brains were processed and sectioned with a cryostat (Microm model HM 505E, Waldorf, Germany) in the parasagittal plane at a thickness of 50 μm, as previously described (Bird et al., 2018). Floating sections were stored at −20 °C in a cryoprotectant solution composed of 0.05 M phosphate buffer pH 7.4, 25% glycerol and 25% ethylene glycol. Sections containing the ventral RSC (equivalent to lateral 0.24–1.32 mm sections of adult mice (Paxinos and Franklin, 2013; Fig 1A)) were processed as described below. Two-dimensional cell counting methods analogous to those of Smiley et al. (2015) were utilized for cell density analyses, as these authors found that 2-dimensional and 3-dimensional cell counting methods revealed comparable reductions in interneuron density following P7 ethanol exposure.

2.3.1. Activated Caspase-3 Immunohistochemistry (IHC)—Four randomly-selected parasagittal sections (50 μm) containing the ventral RSC of 5–6 mice collected at different time points (control and end of exposure; as well as 2, 4, and 8 h post-exposure) were incubated for 2 h in PBS containing 1% bovine serum albumin (Sigma-Aldrich), 0.2% Triton X-100 (Sigma-Aldrich), and 5% donkey serum (Jackson ImmunoResearch, West Grove, PA). Sections were then incubated with rabbit anti-cleaved caspase-3 antibody (1:400 dilution; cat #9661, Cell Signaling, Danvers, MA) for 72 h at 4 °C followed by incubation with donkey anti-rabbit IgG Alexa Fluor™ 555 antibody (1:1000 dilution; cat# A-31572, ThermoFisher, Waltham, MA) for 2 h at 22–24 °C. Tissue sections were next incubated for

20 minutes with 600 nM 4'6-diamidino-2-phenylindole hydrochloride (DAPI, Sigma-Aldrich), rinsed with PBS, mounted on Superfrost Plus microscope slides (VWR, Radnor, PA) with Fluoromount G mounting media (Southern Biotech, Birmingham, AL) and covered with glass coverslips (VWR).

Sections were imaged on a Nuance spectral imaging system (PerkinElmer, Hopkinton, MA) using a Nikon TE-200 U inverted fluorescence microscope, as described elsewhere (Bird et al., 2018). The number of Venus-VGAT positive cells (maximum emission 528 nm, pseudocolored green), the number of activated caspase-3 positive cells (maximum emission of Alexa Fluor™ 555 secondary antibody is 580 nm; pseudocolored red), and the number of Venus-VGAT positive cells co-stained for activated caspase-3 were exhaustively counted in each section in a blind fashion. Quantification was performed using Fiji (NIH Image J software) (Schneider et al., 2012). Images requiring more than one field of view were stitched together using the Grid/Collection stitching plugin in Fiji (Preibisch et al., 2009). Cortical layers I, II-IV and V (Fig 1) were outlined using the polygon selection tool and individual cells were marked using the multipoint selection tool. The area of each cortical layer was recorded, and the density of cells per mm^2 was calculated in each parasagittal section. These results were then averaged together for each animal.

2.3.2. Terminal deoxynucleotidyl transferase dUTP nick end labeling (TUNEL)

—Four randomly collected tissue sections through the ventral RSC from 6 control and 6 8-h post-exposure mice were used for TUNEL, which was performed with the Click-iT™ Plus TUNEL Assay Kit, with Alexa Fluor™ 594 (Catalog #C10618, ThermoFischer, Waltham, MA) following the manufacturer's instructions (Pub. No. MAN0010877) with the exception that after the 15-min fixation in 4% paraformaldehyde, the sections were permeabilized with 0.2% Triton X-100 in PBS for 30 min at room temperature. After incubation with the Click-iT TUNEL reaction mixture for 30 min at 37 °C, the sections were washed with 3% bovine serum albumin in PBS followed by a rinse in PBS. Sections were then incubated with DAPI and mounted as described above. Microscopy and cell density analyses were performed as described above, adjusting for the Alexa Fluor™ 594 emission spectrum (Alexa Fluor™ 594 maximum emission 617 nm, pseudocolored red).

2.3.3. PSVue550 staining—

Apoptotic cells were fluorescently labeled with the PSVue®550 fluorescent probe (Bis(zinc(II)-dipicolylamine) conjugated with Texas-red, Catalog #P-1005, Molecular Targeting Technologies, West Chester, PA). This agent selectively binds to anionic phospholipids, particularly phosphatidylserine exposed on cell membranes, which is externalized in the early stages of apoptotic cell death, triggering clearance by phagocytic cells (Mazzoni et al., 2019). The PSVue550 stock solution (1 mM in 20% dimethyl sulfoxide) was prepared according to the manufacturer's instructions. Four randomly collected tissue sections through the ventral RSC from 6 animals from the control and 6 animals from the 8-h post exposure conditions were washed five times using a solution containing 5 mM N-[Tris(hydroxymethyl)methyl]-2-aminoethane sulfonic acid (TES; pH = 7.4) and 145 mM NaCl (TES buffer) and then incubated with PSVue550 (diluted to a concentration of 0.5 μM in TES buffer) for 2 h at room temperature with gentle shaking. After 5 washes with TES buffer, the sections were incubated with DAPI and mounted as

described above. Microscopy and cell density analyses were performed as described above, adjusting for the PSVue550 emission spectrum (PSVue550 maximum emission is 615 nm, psuedocolored red).

2.4. Slice electrophysiology

Unless otherwise indicated, all chemicals used in these experiments were obtained from Sigma-Aldrich (St. Louis, MO). Venus-VGAT pups (P6–8) were deeply anesthetized with isoflurane (Piramal Critical Care, Bethlehem, PA) and sacrificed by rapid decapitation. Brains were rapidly removed and immersed for 3 min in a solution containing (in mM): 164 sucrose (VWR), 2.5 KCl, 1.25 NaH_2PO_4, 30 $NaHCO_3$, 20 glucose, 25 HEPES, 2 thiourea (Alfa Aesar, Ward Hill, MA), 3 sodium pyruvate, 10 $MgSO_4$, 0.5 $CaCl_2$, and 5 ascorbic acid saturated with 95% O_2/5% CO_2 (pH 7.3–7.4 with KOH; 300–310 mOsm). Coronal brain slices (300 μm) containing the ventral RSC (equivalent to bregma −1.31 to −2.53 sections from adult mice according to the atlas of Paxinos and Franklin (2013); Fig 1B) were prepared using a vibrating slicer (VT 1000 S, Leica Microsystems, Bannockburn, IL, USA). Slices were placed in a holding solution containing (in mM): 95 NaCl, 2.5 KCl, 1.25 NaH_2PO_4, 30 $NaHCO_3$, 20 glucose, 25 HEPES, 2 thiourea, 3 sodium pyruvate, 1 $MgSO_4$, 2 $CaCl_2$, and 5 ascorbic acid saturated with 95% O_2/5% CO_2 (pH 7.3–7.4 with NaOH; 300–310 mOsm) for 40 min at 34–36 °C followed by storage in the same solution at room temperature (approximately 24 °C) for at least 30 min in a slice holding chamber that circulates the oxygenated solution (Model # BSC-PC, Warner Instruments, Hamden, CT). Slices were prepared from animals exposed to ethanol vapor immediately following the 4 h exposure session, and recordings were performed 0–3 h after the recovery procedure described above.

Slices were transferred to a recording chamber that allows the solution to flow above and below the tissue (large bath chamber with slice support, model # RC-27L, Warner Instruments). Recordings were obtained in artificial cerebrospinal fluid (ACSF) containing (in mM): 125 NaCl, 2 KCl, 1.3 NaH_2PO_4, 26 $NaHCO_3$, 10 glucose, 2 $CaCl_2$, 1 $MgSO_4$, and 0.4 ascorbic acid. The chamber was heated to a temperature of 32 °C with a dual automatic temperature controller (Model TC-344B) that was also connected to an in-line solution heater (Model SH-27B) (Warner instruments). Slices were stabilized with platinum wires (Catalog #43288, Alfa Aesar). Neurons were visualized using a BX51WI fixed-stage upright microscope (Olympus, Center Valley, PA) mounted on a manual X-Y translator (Model MT-500, Sutter Instruments, Novato, CA) and equipped with infrared and epifluorescence (mercury arc lamp) illumination, as well as differential interference contrast optics. Venus-positive interneurons were identified using an excitation filter ET470/40x, beam splitter T495lpxr, and emission filter ET525/50m (Chroma Technology Corp. Bellows Falls, VT). Real-time images were acquired with a complementary metal-oxide semiconductor digital camera (Model 01-ROL-BOLT-M-12, Q-Imaging, Surrey, Canada) using Plan 4x (0.10 N.A.) and LUMPlan Fl/IR 40x water immersion (0.8 N.A) lenses (Olympus). Patch pipettes were pulled from filament-containing borosilicate capillary glass (O.D. 1.5 mm; I.D. 0.86 mm, catalog # BF150–86-10; Sutter) with a DMZ Universal Electrode Puller (Zeitz-Instruments Vertriebs GmbH, Martinsried, Germany). Recording electrodes were positioned using a micromanipulator (Model ACCi UI, Scientifica, Clarksburg, NJ). The electrode tip

resistances were 2–3 MΩ. A concentric bipolar stimulating electrode (Catalog # CBAEC75, FHC, Bowdoin, ME) was positioned using an MP-225 micromanipulator (Sutter). Recordings were performed with Axopatch 200B or Multiclamp 700B amplifiers connected to analog-to-digital signal converters (Axon Digidata model 1322A or 1550B, respectively) using Clampex software (version 10 or 11, Molecular Devices, Sunnyvale, CA). Data were acquired at 10 kHz and filtered at 2–4 kHz. Only recordings where the access resistance changed < 20% were kept for analysis. Except when indicated, all recordings were analyzed offline using Clampfit (version 10 or 11) (Molecular Devices).

For whole-cell patch-clamp recordings of electrically-evoked excitatory postsynaptic currents (EPSCs), we used an internal solution containing (in mM): 140 Cs-methanesulfonate, 0.5 EGTA, 15 HEPES, 2 tetramethylammonium chloride, 2 Mg-ATP, 0.3 Na-GTP, and 10 phosphocreatine disodium salt, pH 7.25 (adjusted with CsOH) and 305 mOsm. Neurons were allowed to equilibrate with the internal solution for at least 5 min prior to beginning a recording. Submaximal EPSCs were evoked with a Master-8 pulse stimulator connected to an ISO-Flex stimulus isolator (AMPI, Jerusalem, Israel) every 30 s using 75 μs square pulses (20–200 μA) at a holding potential of −70 mV. The stimulating electrode was located in layer II, approximately 100 μm from the recorded cell (Fig 1B). Non-NMDA EPSCs were recorded in ACSF containing gabazine (25 μM; Hello Bio, Princeton, NJ) and DL-AP5 (50 μM; Hello Bio), and were verified by blocking at the end of recording with NBQX (10 μM; Tocris, Minneapolis, MN). For paired-pulse experiments, the inter-pulse interval was 50 ms. For NMDA EPSC recordings, the ACSF contained zero $MgSO_4$, $CaCl_2$ (3 mM), gabazine (25 μM), and NBQX (10 μM), and we confirmed that the events were NMDA receptor-mediated by blocking them at the end of recording with DL-AP5 (50 μM). Solutions were bath-applied to the recording chamber at a rate of 2 ml/min using a peristaltic pump (Master Flex, model 7518–10, Cole-Parmer, Vernon Hills, IL), including ethanol-containing solutions (made from 95% spectrophotometric grade ethanol, catalog number 493511, Sigma-Aldrich). The last 3 min of each phase (baseline, acute ethanol, wash) were analyzed to determine the overall effect of ethanol with respect to the average of control and washout responses.

Spontaneous, miniature EPSCs (mEPSCs) were recorded in the presence of tetrodotoxin (0.5 μM, Abcam, Cambridge, MA). Five min of mEPSC recordings were analyzed using the Mini Analysis Program (Synaptosoft, Decatur, GA). The average event amplitude, frequency, and decay constant tau were calculated for both pyramidal neurons and interneurons before and after vapor chamber exposure. The decay constant tau was calculated by fitting a single exponential decay curve to the average mEPSC waveform from each cell.

The whole-cell current-clamp configuration was also used to measure action potential firing in response to current injection. Current was injected into pyramidal neurons and interneurons to maintain the membrane potential near −70 mV. Intrinsic firing properties were analyzed by injecting currents ranging from 200–600 pA in 200 pA increments, and the instantaneous firing frequency was measured. Synaptically-evoked action potentials were generated using the concentric bipolar stimulating electrode placed in layer II as described above, using a modification of methods described previously (Carta et al., 2003). Briefly,

action potentials were evoked with trains of 5 stimuli at 20 Hz, using stimulation intensities of 20–200 μA. Stimulation intensity was adjusted to evoke an action potential at all 5 stimuli under baseline conditions before drugs were applied. We used an internal solution containing (in mM): 140 K-methanesulfonate, 0.5 EGTA, 15 HEPES, 4 KCl, 2 Mg-ATP, 0.3 Na-GTP, and 10 phosphocreatine disodium salt, pH 7.25 (adjusted with KOH) and 305 mOsm. The ACSF did not contain any antagonist of neurotransmitter receptors. For action potential analyses, action potential numbers during the last 5 min of each 10 min phase (baseline, drug application, and washout) were quantified. For all electrophysiology experiments, only one cell was recorded from each slice.

2.5. Statistical Analysis

Statistical analyses were performed using Prism version 8.2.0 (GraphPad Software, San Diego, CA) and SPSS version 26 (IBM, Armonk, NY). The unit of determination (n) for BEC, IHC, and electrophysiology assays performed before and after vapor chamber exposure was a single animal (no more than two animals/litter were used per data point to minimize litter effects). For electrophysiology experiments examining how acute bath application of ethanol administration affected excitability, the unit of determination was a single cell (the same was the case for all experiments on the effects of glutamate ionotropic receptor antagonists). Data sets analyzed using two-independent sample or one-independent sample tests were tested for normality using a Shapiro-Wilkes test. Normally distributed data were analyzed using an unpaired t-test (with Welch's correction for unequal variances when necessary) or a one-sample t-test (comparing to 0), while non-normal data were analyzed using a Mann-Whitney U test or a Wilcoxon signed-rank test (compared to 0). For data analyzed using analyses of variance (ANOVA), residuals were tested for normality using the Shapiro-Wilkes test, and equality of variances was tested using Levene's test. Data that passed these tests ($p > 0.05$) were analyzed using one-way or factorial ANOVA (repeated measures when necessary, with Greenhouse-Geisser corrected p-values and F-ratios when assumptions of sphericity were violated) followed by multiple comparison post-hoc tests. One-way ANOVA data that failed these tests were analyzed using the non-parametric Kruskal-Wallis test followed by Dunn's multiple comparison test. Two-Way ANOVA data that violated these tests were analyzed using two different non-parametric tests. Main effects were examined using the Scheirer-Ray-Hare test (Scheirer et al., 1976), and interactions between factors were analyzed using the Adjusted Rank Transform test (Leys and Schumann, 2010). Post-hoc multiple comparisons were performed using data transformed with the Scheirer-Ray-Hare test, and groups were compared using Dunn's test when comparing more than two groups, or a Mann-Whitney U test when comparing two groups. All post-hoc p-values were corrected using a Bonferroni correction for the number of comparisons made. Effect sizes are reported as follows: partial eta squared (η_p^2) for ANOVAs, Adjusted Rank Transform interactions, and Kruskal-Wallis tests; eta squared (η^2) for Scheirer-Ray-Hare main effects; Hedges' g for t-tests and parametric multiple comparisons; and r for Dunn's post-hoc tests, Mann-Whitney U tests, and Wilcoxon signed-rank tests. Data are presented as group means and standard error of the means. We report precise p-values, as recommended in a recent article (Amrhein et al., 2019). A comprehensive collection of all statistical analyses can be found in Supplemental Table 1.

3. Results

3.1. Ethanol concentration in pup blood

Ethanol vapor chamber exposure for 4 h at P7 produced pup peak BECs near 80 mM (0.36 g/dl; for comparison, the legal intoxication limit in the U.S.A. is 17.4 mM = 0.08 g/dl). Pup BECs were elevated for several hours following the cessation of vapor chamber exposure (Fig 2; see Supplementary Table 1 for results of statistical analyses). The BECs followed a time course similar to the one reported by Olney and collaborators (Ikonomidou et al., 2000).

3.2. Ethanol vapor exposure at P7 triggered apoptotic cell death

The impact of exposure to ethanol vapor at P7 on RSC neuronal viability was initially assessed using IHC for cleaved caspase-3. Fig 3A–H show representative images of brain sections from control (non-exposed) and ethanol exposed pups euthanized at different time points post-exposure. Fig 3I–J show that ethanol exposure induced a time- and layer-dependent increase in the density of cleaved caspase-3 positive cells (Adjusted rank transform interaction $F(8,63) = 5.185$, $p < 0.0001$, $\eta_p^2 = 0.397$), as well as density of GABAergic interneurons that were positive for both cleaved caspase-3 and Venus (Adjusted rank transform interaction $F(8,63) = 3.880$, $p = 0.0009$, $\eta_p^2 = 0.330$) (see Supplemental Table 1 for detailed results of two-way nonparametric analyses for all apoptosis experiments). The density of cleaved caspase-3 positive cells increased 4 h and 8 h after the end of ethanol vapor exposure in layers II-IV (4 h $p = 0.0044$, $r = 1.033$; 8 h $p = 0.0015$, $r = 1.074$) and in layer V (4 h $p = 0.025$, $r = 0.863$; 8 h $p < 0.0001$, $r = 1.280$ by Dunn's post-hoc test; Fig 3I). The density of interneurons that were positive for both cleaved caspase-3 and Venus also increased 4 h and 8 h after the end of exposure in layers II-IV (4 h $p = 0.0077$, $r = 0.981$; 8 h $p = 0.016$, $r = 0.868$), as well as 2, 4, and 8 h after the end of exposure in Layer V (2 h $p = 0.010$, $r = 0.954$; 4 h $p = 0.025$; $r = 0.863$; 8 h $p = 0.0017$; $r = 1.063$ by Dunn's post hoc test; Fig 3J) (Supplemental Fig 1 shows high magnification colocalization images for all apoptosis experiments).

We confirmed that P7 ethanol vapor exposure causes apoptotic cell death using TUNEL and PSVue staining. We focused on the 8 h time point because this is when the largest effects were observed in the activated caspase-3 IHC experiments. Fig 4A–H show representative images of TUNEL-stained brain sections from control and ethanol exposed pups euthanized 8 h post-exposure. Fig 4I–J show that ethanol exposure induced a layer-dependent increase in the density of TUNEL positive cells (Adjusted rank transform interaction $F(2,30) = 16.215$, $p < 0.0001$, $\eta_p^2 = 0.519$), as well as density of cells that were positive for both TUNEL and Venus (Adjusted rank transform interaction $F(2,30) = 5.149$, $p = 0.012$, $\eta_p^2 = 0.256$). The density of TUNEL positive cells increased 8 h after the end of ethanol vapor exposure in layers II-IV and layer V ($p = 0.0066$, $r = 0.832$ for both layers II-IV and layer V using Mann-Whitney U tests). The density of interneurons that were positive for both TUNEL and Venus also increased 8 h after the end of exposure in layer I, layers II-IV and layer V ($p = 0.0066$, $r = 0.832$ for layer I, layers II-IV and layer V using Mann-Whitney U tests). Fig 5A–H show representative images of PSVue-stained brain sections from control and ethanol exposed pups euthanized 8 h post-exposure. Fig 5I–J show that ethanol exposure

induced a layer-dependent increase in the density of PSVue positive cells (Adjusted rank transform interaction $F(2,30) = 44.306$, $p < 0.0001$, $n_P^2 = 0.747$), as well as density of interneurons that were positive for both PSVue and Venus (Adjusted rank transform interaction $F(2,30) = 19.027$, $p < 0.0001$, $\eta_P^2 = 0.559$). The density of PSVue positive cells was increased 8 h after the end of ethanol vapor exposure in layer I, layers II-IV and layer V ($p = 0.0066$, $r = 0.832$ for layer I, layers II-IV and layer V using Mann-Whitney U tests). The density of cells that were positive for both PSVue and Venus also increased 8 h after the end of exposure in layer I, layers II-IV, and layer V ($p = 0.0066$, $r = 0.832$ for layer I, layers II-IV and layer V using Mann-Whitney U tests).

3.3. Effect of ethanol on glutamatergic excitatory postsynaptic currents

Others have postulated that ethanol triggers apoptosis of developing neurons, in part, via inhibition of NMDA receptors. Therefore, we assessed the acute effect of bath-applied ethanol on NMDA receptor-mediated EPSCs in brain slices from P6–8 pups. For comparison, we also measured its effect on non-NMDA EPSCs. We focused on pyramidal neurons and interneurons located in layer V of the RSC because this area is particularly sensitive to ethanol-induced apoptotic cell death (Figs 3–5). We chose an ethanol concentration (90 mM) that is near the peak BEC produced by the vapor ethanol exposure paradigm (Fig 2). To determine if the receptors develop acute tolerance to ethanol's effects, we tested the acute effect of bath-applied ethanol in slices prepared before and immediately after the 4-h *in vivo* ethanol vapor chamber exposure.

We first measured the effect of vapor chamber exposure on electrically evoked EPSCs. Vapor chamber exposure did not affect the membrane resistance or capacitance of pyramidal neurons or interneurons and did not alter the properties of electrically-evoked NMDA or non-NMDA receptor EPSCs (Table 1). Acute bath application of ethanol inhibited NMDA EPSCs to a similar extent in both control slices and slices from pups exposed to ethanol vapor for 4 h (Fig 6A–D). Exposure to 90 mM ethanol reduced the NMDA EPSC by 20.6 ± 3.4% in pyramidal neurons from control mice, whereas pyramidal neurons from mice exposed to ethanol vapor showed a 13.7 ± 4.8% reduction (Fig 6A, C). In interneurons from control mice, 90 mM ethanol reduced the NMDA EPSC by 17.8 ± 8.3%; while interneurons from mice exposed to ethanol vapor showed a 25.5 ± 9.3% reduction (Fig 6B, D). Three-way repeated measures ANOVA of the effect of acute bath application of ethanol X neuronal type X vapor chamber exposure condition indicates that the acute effect of ethanol on percent inhibition of NMDA EPSC amplitude was similar in pyramidal neurons and interneurons (acute ethanol X cell type interaction $p = 0.14$).

Acute bath application of ethanol inhibited non-NMDA EPSCs to a similar extent in both control slices and slices from pups exposed to ethanol vapor for 4 h (Fig 6E–H). In pyramidal neurons from control mice, 90 mM ethanol reduced the non-NMDA EPSC by 23.1 ± 6.4%; the same treatment reduced it by 14.1 ± 4.6% in pyramidal neurons from mice exposed *in vivo* to ethanol vapor (Fig 6E, G). In interneurons from control mice, acute bath application of 90 mM ethanol reduced the non-NMDA EPSC by 8.4 ± 5%; in interneurons from mice exposed *in vivo* to ethanol vapor, it reduced it by 6.3 ± 4.6% (Fig 6F, H). Three-way repeated measures ANOVA of the effect of acute bath application of ethanol X neuronal

type X vapor chamber exposure condition indicates that the acute effect of bath-applied ethanol on percent inhibition of non-NMDA EPSC amplitude was similar in pyramidal neurons and interneurons (acute ethanol X cell type interaction p = 0.98). We also measured the effect of acute bath application of ethanol on paired-pulse plasticity (Supplemental Fig 2). Using three-way repeated measures ANOVA, we found an effect of exposure phase (baseline vs. acute bath application of ethanol vs. wash) on paired pulse ratio ($F(2,50) = 5.256$, $p = 0.0085$, $\eta_p^2 = 0.174$) but no other main effects of cell type, vapor chamber exposure condition, or interaction between these factors (all p's > 0.16). Overall, there was no difference in paired-pulse ratios between the baseline and acute bath application of ethanol conditions (post-hoc multiple comparison $t(50) = 1.560$, $p = 0.38$, $g = 0.230$, or between the baseline and washout conditions ($t(50) = 1.682$, $p = 0.30$, $g = 0.214$). There was an overall increase in paired-pulse ratio between the acute bath application of ethanol and washout ($t(50) = 3.242$, $p = 0.0064$, $g = 0.482$).

To further assess the effect of ethanol vapor chamber exposure on glutamate release, we measured its effect on spontaneous mEPSCs (Supplemental Fig 3). In pyramidal neurons, vapor chamber exposure led to an increase in the amplitude of mEPSCs (Welch's unpaired t-test $t(8.545) = 1.935$, $p = 0.087$, $g = 0.865$) and a decrease in the decay constant tau (Mann-Whitney U test ($n1 = 7$, $n2 = 9$), $p = 0.016$, $r = 0.596$). In pyramidal neurons there was no effect of vapor chamber exposure on the frequency of mEPSCs (p > 0.26). There was no effect of vapor chamber exposure on the amplitude, frequency, or decay constant tau in interneurons (all p's > 0.21).

3.4. Effect of ethanol on action potential firing

We investigated if the effect of ethanol on NMDA and/or non-NMDA EPSCs was sufficient to reduce action potential firing in response to synaptic stimulation. To maximize the induction of action potential firing, EPSPs were evoked by trains of 5 stimuli at 20 Hz (Fig 7). The EPSPs and associated action potentials were abolished by co-application of 100 μM DL-AP5 and 10 μM NBQX (n = 4 cells; not shown). In pyramidal neurons, application of 90 mM ethanol reduced action potential firing by 82.7 ± 7.8% (Fig. 7A, C). In interneurons, application of 90 mM ethanol reduced action potential firing by 40.2 ± 7.7% (Fig. 7B, D). Acute bath application of ethanol inhibited action potential firing to a greater degree in pyramidal neurons than in interneurons (repeated measures two-way ANOVA acute exposure X cell type interaction: $F(1,20) = 14.860$, $p = 0.0010$, $\eta_p^2 = 0.426$). Acute ethanol application did not reduce intrinsic action potential firing evoked by current injection in pyramidal neurons or interneurons (Supplementary Fig 4).

To assess the contribution of ethanol-induced inhibition of NMDA and non-NMDA receptors to their effects on action potential firing evoked by synaptic stimulation, we determined the concentrations of DL-AP5 and NBQX that inhibit the NMDA and non-NMDA EPSCs, respectively, to a similar extent as 90 mM ethanol (Supplemental Fig 5). These concentrations were 5 μM for DL-AP5 (24.6 ± 2.2% inhibition from control) and 50 nM for NBQX (30.3 ± 4.1% inhibition from control). We then compared synaptically-evoked action potential firing after acute bath application of either: 90 mM ethanol (calculated from data shown in Fig 6), 5 μM DL-AP5, 50 nM NBQX, or 5 μM DL-AP5 and

50 nM NBQX. In pyramidal neurons, we found that 5 μM DL-AP5 reduced synaptically-evoked action potential firing less than 90 mM ethanol; 50 nM NBQX had little effect; and the combination of 5 μM DL-AP5 and 50 nM NBQX reduced action potential firing to a similar extent as 90 mM ethanol (Fig 7A–C). In interneurons, we found that 5 μM DL-AP5 reduced synaptically-evoked action potential firing to a similar extent as 90 mM ethanol; 50 nM NBQX had little effect; and the combination of 5 μM DL-AP5 and 50 nM NBQX reduced action potential firing to a similar extent as 90 mM ethanol (Fig 7B–D).

4. DISCUSSION

The findings of this study increase our understanding of the mechanisms underlying the increase in apoptotic neurodegeneration caused by binge-like exposure to high doses of ethanol during the third trimester equivalent of human pregnancy. Our results suggest that inhibition of NMDA receptors can explain, in part, ethanol-induced inhibition of neuronal excitability in the RSC. Inhibition of NMDA receptors by ethanol may be a critical component of the mechanism explaining why cells undergo apoptosis during this critical developmental period. In addition, these findings reveal potential approaches for therapeutic interventions that may ameliorate ethanol-induced death of neurons during late stages of fetal development or in preterm infants.

The vapor exposure paradigm used here resulted in BECs that were above the previously reported toxic threshold (200 mg/dl or 44 mM) for the induction of apoptotic neurodegeneration in postnatal rodents (Ikonomidou et al., 2000; Olney et al., 2002). The BECs followed a similar time course to that reported by Ikonomidou (2000) in P7 rats injected with ethanol subcutaneously, with the exception that levels increased more slowly in the vapor chamber paradigm. At the time point where the number of apoptotic cells was the highest (8 h after the end of the 4-h exposure), ethanol was still present in the pup blood at levels higher than the toxic threshold. Our vapor chamber exposure paradigm produced a similar increase in apoptosis to that observed in rodent pups that received alcohol via subcutaneous injections (Ikonomidou et al., 2000) or gavage (Jiang et al., 2007). Ikonomidou et al (2000) found a 35-fold increase in the density of degenerating cells in RSC layers II and IV of P7 rats. Saito (2007) found a similar increase in the density of activated caspase-3 positive cells in the RSC of P7 mice. In general agreement with these reports, we observed a 32-fold and 88-fold increase in the density of activated caspase-3 positive cells 8 h after the end of ethanol vapor chamber exposure in RSC layers II-IV and layer V of Venus-VGAT mice, respectively. The number of activated caspase-3 positive interneurons was increased by 17- and 29-fold in RSC layers II-IV and layer V, respectively. Similar results were obtained with two other apoptotic assays: PSVue and TUNEL staining. Our results demonstrating enhanced vulnerability of layer V cells to ethanol-induced apoptosis are consistent with those of previous studies (Lebedeva et al., 2017; Olney et al., 2002; Toesca et al., 2003). Given that layer V is the major output layer of the cerebral cortex, it is possible that loss of either local inhibitory interneurons or pyramidal neurons in the RSC that project to other brain regions could have significant functional impacts on parahippocampal network activity (Sugar et al., 2011), which could partially explain learning and memory deficits observed following developmental exposure to ethanol. These findings are also consistent with recent results indicating that subcutaneous ethanol administration produces a long-

lasting decrease in the number of parvalbumin-positive interneurons and perineuronal net-positive cells in the murine RSC (Lewin et al., 2018; Saito et al., 2019). We did not specifically ascertain that parvalbumin-positive interneurons underwent apoptosis in this study, as our use of Venus-VGAT mice did not allow us to differentiate between subtypes of interneurons. A more rigorous examination of specific interneuron subtype vulnerability in the RSC and other brain regions is warranted, as others have demonstrated region-specific alterations in interneuron subtype survival following ethanol exposure during development (Coleman et al., 2012; Smiley et al., 2015). Moreover, future studies should also investigate if RSC interneurons are affected by first and/or second trimester-equivalent ethanol exposure, which has been shown to reduce the number of cortical GABAergic interneurons (Bailey et al., 2004; Miller, 2006; Moore et al., 1998; Moore et al., 1997) as well as cause premature tangential migration of these cells into the cerebral cortex (Cuzon et al., 2008; Skorput et al., 2015). Taken together, our findings indicate that the RSC is an important target of third trimester-equivalent ethanol exposure and whether this effect can also be caused by ethanol exposure during other periods of gestation or has long-term behavioral consequences deserves further investigation.

Vapor chamber exposure for 4 h did not affect the properties of NMDA EPSCs, suggesting that the phosphorylation state, surface expression, or subunit composition of the receptors were not altered. NMDA EPSCs in RSC layer V pyramidal neurons and interneurons were acutely inhibited by bath-applied ethanol to a similar extent as has been found in other electrophysiological studies with slices from neonatal rodents, including field excitatory postsynaptic potential recordings from rat (Puglia and Valenzuela, 2010) and murine (Gordey et al., 2001) CA1 hippocampal pyramidal neurons. The magnitude of acute ethanol-induced inhibition of NMDA EPSCs is also in general agreement with that observed in slices from older rodents (Lovinger et al., 1990; Miyakawa et al., 1997; Swartzwelder et al., 1995; Yaka et al., 2003). Importantly, we found no evidence of acute tolerance development, as NMDA EPSCs displayed similar sensitivity to acute ethanol exposure before and after the 4-h ethanol vapor exposure. This finding indicates that the mechanisms involved in rapid NMDA receptor tolerance to ethanol (e.g., tyrosine kinase- and/or metabotropic glutamate receptor-dependent mechanisms (Li et al., 2005; Miyakawa et al., 1997; Petit-Paitel et al., 2012)) are not active in RSC layer V pyramidal neurons during postnatal development. This could be due to lack of expression of scaffolding proteins (e.g., RACK1) that link Fyn kinase to the GluN2B subunit, which would not allow it to phosphorylate this subunit and develop acute tolerance to ethanol (Reviewed in (Ron and Wang, 2009)). Alternatively, it is possible that NMDA receptors did develop tolerance to ethanol but that they re-sensitized during slice preparation and/or recovery, or that repeated exposures to ethanol are required for long-lasting tolerance development. Moreover, based on changes in NMDA EPSC decay, we cannot eliminate the possibility that subunit expression was altered by vapor chamber ethanol exposure. Future studies will need to use specific GluN2A and GluN2B receptor antagonists to determine the contribution of these subunits to EPSC characteristics in naïve and vapor chamber exposed animals.

As was the case for NMDA EPSCs, vapor chamber ethanol exposure affected neither the properties of evoked non-NMDA EPSCs nor their sensitivity to bath-applied ethanol exposure in both pyramidal cells and interneurons of the RSC. We did find that vapor

chamber exposure moderately increased mEPSC amplitude and significantly decreased the mEPSC decay constant tau in pyramidal neurons. These results indicate that non-NMDA receptor subunit composition may be altered by ethanol exposure; if persistent, this effect would be consistent with AMPA receptor alterations observed in other studies (Bellinger et al., 2002; Dettmer et al., 2003). However, we did not observe changes in evoked EPSC decay, suggesting that alterations in subunit composition may selectively occur at a subpopulation of non-NMDA receptors in pyramidal neurons. The finding that RSC-evoked non-NMDA EPSCs are acutely inhibited by bath-applied ethanol is consonant with the results of a previous study from our laboratory demonstrating a similar reduction in the amplitude of AMPA receptor-mediated field excitatory postsynaptic potentials in the CA1 hippocampal region of neonatal rats (Puglia and Valenzuela, 2010). However, acute ethanol did not affect the frequency or amplitude of AMPA receptor-mediated spontaneous EPSCs in layer II/IM pyramidal neurons of the developing rat neocortex, suggesting that its effects on these receptors could be species specific (Sanderson et al., 2009). Our finding that ethanol vapor chamber exposure did not alter paired-pulse plasticity or mEPSC frequency in RSC pyramidal neurons and interneurons indicates that it does not act via an effect on the probability of glutamate release. These results suggest that ethanol modulates NMDA and non-NMDA receptor function at the postsynaptic level, in agreement with previous findings in the CA1 region of the rat hippocampus (Puglia and Valenzuela, 2010). We previously found that ethanol inhibits both AMPA and NMDA EPSCs via a presynaptic mechanism in CA3 hippocampal pyramidal neurons from neonatal rats (Mameli et al., 2005). Therefore, the mechanism of action of ethanol on glutamatergic transmission in developing neurons appears to be dependent on the brain region examined.

Acute ethanol exposure-induced inhibition of ionotropic glutamate receptors in developing RSC neurons is likely to produce impairments in synaptic plasticity (Granato and Dering, 2018). Puglia and Valenzuela (2010) showed that bath application of 80 mM ethanol inhibits the induction of long-term potentiation in the CA1 hippocampal region of P7–9 rats. If ethanol has a similar effect in the RSC, this is likely to have a deleterious impact on the maturation of neuronal networks and integrate with its effects on neuronal survival. Developing synapses are functionally labile, which makes them susceptible to activity-dependent processes that determine their elimination or stabilization driven, in part, by rhythmic network activity (Hanse et al., 2009). Therefore, future experiments should determine if ethanol exposure during the third trimester-equivalent inhibits Hebbian synaptic plasticity in the RSC, disrupting the processes that regulate synaptic refinement (Fernandes and Carvalho, 2016; Henson et al., 2017; Hlushchenko et al., 2016; Ziburkus et al., 2009). As recently reviewed by Granato and Dering (2018), ethanol inhibition of synaptic plasticity not only contributes to its apoptotic effects but also causes excitation/inhibition imbalances in surviving neurons, leading to abnormal formation of neuronal circuits and long-lasting neurobehavioral changes.

A key finding of our study is that bath-applied ethanol exposure strongly reduced action potential firing evoked by synaptic stimulation in RSC pyramidal neurons. In addition, a rebound increase in firing was observed in these cells upon ethanol washout. In interneurons, both the inhibition of firing and rebound increase in firing were less pronounced and the inhibition of firing developed more gradually. Our experiments with submaximal

concentrations of DL-AP5 and NBQX to mimic the effects of ethanol on NMDA and AMPA current amplitude, respectively, suggest that inhibition of NMDA EPSCs (but not non-NMDA EPSCs) by ethanol can partially explain its effects on synaptically-evoked firing in pyramidal neurons. In interneurons, NMDA receptor inhibition may be solely responsible for acute ethanol's actions. Whether or not partial inhibition of NMDA receptors directly causes apoptosis of neurons at P7 via a decrease in neuronal firing will be the subject of future studies to directly link these actions of ethanol to programmed cell death and to determine the downstream mechanisms responsible for the pro-apoptotic effects of NMDA receptor inhibition (e.g., inhibition of activity-dependent BDNF release and phosphatidylinositol 3-kinase/Akt pathway activation (Golbs et al., 2011; Heck et al., 2008; Kirischuk et al., 2017)). Although Ikonomidou et al. (2000) found that intraperitoneal injection of NBQX did not mimic the apoptotic response elicited by ethanol injection in P7 rat pups, a role of non-NMDA receptors in this process cannot be completely ruled out, as caspase-mediated breakdown of AMPA receptor subunits has been shown to trigger apoptotic neurodegeneration (Lu et al., 2001). However, our data suggests that the magnitude of ethanol-induced inhibition of AMPA receptor function is not sufficient to reduce neuronal excitability and trigger apoptosis via this mechanism. Therefore, additional mechanisms are likely to be involved in the reduction in excitability, particularly in pyramidal neurons, with an increase in $GABA_a$ receptor-mediated inhibition being a likely possibility. It should be considered that $GABA_a$ receptors exert excitatory actions in developing neurons in brain slices that can be potentiated by ethanol (Galindo et al., 2005); nevertheless, these *in vitro* findings may not be relevant *in vivo,* where $GABA_a$ receptors can exert inhibitory effects on developing neuronal networks (Kirmse et al., 2015; Valeeva et al., 2016). Another possibility is that ethanol acutely inhibits synaptically-evoked firing of pyramidal neurons via modulation of potassium channels and other ion channels (Bodhinathan and Slesinger, 2014; Dopico et al., 2016; Harrison et al., 2017; You et al., 2019). However, our finding that ethanol did not affect action potential firing evoked by current injection suggests that changes in intrinsic excitability are less likely to play a role in its inhibitory actions on RSC developing neurons.

Taken together with previous studies (Creeley and Olney, 2013; Granato and Dering, 2018; Saito et al., 2016), our findings suggest that agents that positively modulate NMDA receptor function (e.g., sulfated steroids, oxysterols and D-cycloserine) (Cioffi, 2013; Hackos and Hanson, 2017) could ameliorate neurodegeneration induced by heavy, binge-like ethanol consumption during late pregnancy. However, these agents would have to be administered during the acute intoxication phase, as studies with neonatal rats suggest that excitotoxicity-mediated by rebound NMDA receptor over-activation during ethanol withdrawal causes behavioral deficits that can be prevented by NMDA receptor antagonists (e.g., memantine and related agents) (Idrus et al., 2014; Lewis et al., 2007; Lewis et al., 2012; Thomas et al., 2001; Thomas et al., 2004). Thus, different approaches would need to be used in late pregnancy to protect the fetal brain from neurodegeneration depending on whether ethanol is still present in the body or if it has been already eliminated. While NMDA receptor dysfunction plays an important role in ethanol-induced apoptotic neurodegeneration during the equivalent to the third trimester of human pregnancy, other mechanisms are likely to contribute to this process (e.g., inflammatory responses, alterations in histone turnover,

increased endoplasmic reticulum stress, and alterations in gene expression (Chastain and Sarkar, 2014; Kleiber et al., 2014; Lewis et al., 2012; Li et al., 2019; Rachdaoui et al., 2017; Subbanna et al., 2018)). Therefore, effective protection of the fetus from ethanol-induced neurotoxicity will likely require a combination of therapeutic interventions aimed at the multiple mechanisms involved in this process.

Supplementary Material

Refer to Web version on PubMed Central for supplementary material.

Acknowledgements

Author contributions: CWB and CFV designed experiments, analyzed data, interpreted findings and wrote the paper; CWB, MJB, GJC, NGF, BJ, and HRP performed experiments and analyzed data. We thank Drs. Kevin Caldwell, Nora Perrone-Bizzozero, Daniel Savage, and Valentina Licheri for critically reading the manuscript.

Funding and Disclosure:

The authors declare no competing financial interests or other conflicts of interest. Supported by NIH grants R37 AA015614 and P50 AA022534 (CFV); Undergraduate Pipeline Network Program and Maximizing Access to Research Career Programs (MB). Unbiased stereology studies were carried out at the University of New Mexico & Cancer Center Fluorescence Microscopy Shared Resource, funded as detailed on: http://hsc.unm.edu/crtc/microscopy/acknowledgement.shtml.

REFERENCES

Akinmboni TO, Davis NL, Falck AJ, Bearer CF, Mooney SM, 2018 Excipient exposure in very low birth weight preterm neonates. J Perinatol 38, 169–174. [PubMed: 29095430]

Amrhein V, Greenland S, McShane B, 2019 Scientists rise up against statistical significance. Nature 567, 305–307. [PubMed: 30894741]

Bailey CD, Brien JF, Reynolds JN, 2004 Chronic prenatal ethanol exposure alters the proportion of GABAergic neurons in layers II/III of the adult guinea pig somatosensory cortex. Neurotoxicol Teratol 26, 59–63. [PubMed: 15001214]

Bellinger FP, Davidson MS, Bedi KS, Wilce PA, 2002 Neonatal ethanol exposure reduces AMPA but not NMDA receptor levels in the rat neocortex. Brain Res Dev Brain Res 136, 77–84. [PubMed: 12036520]

Bird CW, Taylor DH, Pinkowski NJ, Chavez GJ, Valenzuela CF, 2018 Long-term Reductions in the Population of GABAergic Interneurons in the Mouse Hippocampus following Developmental Ethanol Exposure. Neuroscience 383, 60–73. [PubMed: 29753864]

Bodhinathan K, Slesinger PA, 2014 Alcohol modulation of G-protein-gated inwardly rectifying potassium channels: from binding to therapeutics. Front Physiol 5, 76. [PubMed: 24611054]

Carta M, Ariwodola OJ, Weiner JL, Valenzuela CF, 2003 Alcohol potently inhibits the kainate receptor-dependent excitatory drive of hippocampal interneurons. Proc Natl Acad Sci U S A 100, 6813–6818. [PubMed: 12732711]

Chastain LG, Sarkar DK, 2014 Role of microglia in regulation of ethanol neurotoxic action. Int Rev Neurobiol 118, 81–103. [PubMed: 25175862]

Cioffi CL, 2013 Modulation of NMDA receptor function as a treatment for schizophrenia. Bioorg Med Chem Lett 23, 5034–5044. [PubMed: 23916256]

Coleman LG Jr., Oguz I, Lee J, Styner M, Crews FT, 2012 Postnatal day 7 ethanol treatment causes persistent reductions in adult mouse brain volume and cortical neurons with sex specific effects on neurogenesis. Alcohol 46, 603–612. [PubMed: 22572057]

Creeley CE, Olney JW, 2013 Drug-Induced Apoptosis: Mechanism by which Alcohol and Many Other Drugs Can Disrupt Brain Development. Brain Sci 3, 1153–1181. [PubMed: 24587895]

Cudd TA, 2005 Animal model systems for the study of alcohol teratology. Experimental biology and medicine 230, 389–393. [PubMed: 15956768]

Cuzon VC, Yeh PW, Yanagawa Y, Obata K, Yeh HH, 2008 Ethanol consumption during early pregnancy alters the disposition of tangentially migrating GABAergic interneurons in the fetal cortex. J Neurosci 28, 1854–1864. [PubMed: 18287502]

Dettmer TS, Barnes A, Iqbal U, Bailey CD, Reynolds JN, Brien JF, Valenzuela CF, 2003 Chronic prenatal ethanol exposure alters ionotropic glutamate receptor subunit protein levels in the adult guinea pig cerebral cortex. Alcohol Clin Exp Res 27, 677–681. [PubMed: 12711930]

Dopico AM, Bukiya AN, Kuntamallappanavar G, Liu J, 2016 Modulation of BK Channels by Ethanol. Int Rev Neurobiol 128, 239–279. [PubMed: 27238266]

Dukes K, Tripp T, Willinger M, Odendaal H, Elliott AJ, Kinney HC, Robinson F, Petersen JM, Raffo C, Hereld D, Groenewald C, Angal J, Hankins G, Burd L, Fifer WP, Myers MM, Hoffman HJ, Sullivan L, Network P, 2017 Drinking and smoking patterns during pregnancy: Development of group-based trajectories in the Safe Passage Study. Alcohol 62, 49–60. [PubMed: 28755751]

Ethen MK, Ramadhani TA, Scheuerle AE, Canfield MA, Wyszynski DF, Druschel CM, Romitti PA, 2009 Alcohol consumption by women before and during pregnancy. Maternal and child health journal 13, 274–285. [PubMed: 18317893]

Farber NB, Creeley CE, Olney JW, 2010 Alcohol-induced neuroapoptosis in the fetal macaque brain. Neurobiol Dis 40, 200–206. [PubMed: 20580929]

Fernandes D, Carvalho AL, 2016 Mechanisms of homeostatic plasticity in the excitatory synapse. J Neurochem 139, 973–996. [PubMed: 27241695]

Galindo R, Zamudio PA, Valenzuela CF, 2005 Alcohol is a potent stimulant of immature neuronal networks: implications for fetal alcohol spectrum disorder. J Neurochem 94, 1500–1511. [PubMed: 16000153]

Golbs A, Nimmervoll B, Sun JJ, Sava IE, Luhmann HJ, 2011 Control of programmed cell death by distinct electrical activity patterns. Cereb Cortex 21, 1192–1202. [PubMed: 20966045]

Gordey M, Mekmanee L, Mody I, 2001 Altered effects of ethanol in NR2A(DeltaC/DeltaC) mice expressing C-terminally truncated NR2A subunit of NMDA receptor. Neuroscience 105, 987–997. [PubMed: 11530236]

Granato A, Dering B, 2018 Alcohol and the Developing Brain: Why Neurons Die and How Survivors Change. Int J Mol Sci 19.

Hackos DH, Hanson JE, 2017 Diverse modes of NMDA receptor positive allosteric modulation: Mechanisms and consequences. Neuropharmacology 112, 34–45. [PubMed: 27484578]

Hanse E, Taira T, Lauri S, Groc L, 2009 Glutamate synapse in developing brain: an integrative perspective beyond the silent state. Trends Neurosci 32, 532–537. [PubMed: 19733923]

Harrison NL, Skelly MJ, Grosserode EK, Lowes DC, Zeric T, Phister S, Salling MC, 2017 Effects of acute alcohol on excitability in the CNS. Neuropharmacology 122, 36–45. [PubMed: 28479395]

Heaton MB, Paiva M, Madorsky I, Shaw G, 2003 Ethanol effects on neonatal rat cortex: comparative analyses of neurotrophic factors, apoptosis-related proteins, and oxidative processes during vulnerable and resistant periods. Brain Res Dev Brain Res 145, 249–262. [PubMed: 14604765]

Heck N, Golbs A, Riedemann T, Sun JJ, Lessmann V, Luhmann HJ, 2008 Activity-dependent regulation of neuronal apoptosis in neonatal mouse cerebral cortex. Cereb Cortex 18, 1335–1349. [PubMed: 17965127]

Henson MA, Tucker CJ, Zhao M, Dudek SM, 2017 Long-term depression-associated signaling is required for an in vitro model of NMDA receptor-dependent synapse pruning. Neurobiol Learn Mem 138, 39–53. [PubMed: 27794462]

Himes SK, Dukes KA, Tripp T, Petersen JM, Raffo C, Burd L, Odendaal H, Elliott AJ, Hereld D, Signore C, Willinger M, Huestis MA, Prenatal Alcohol in S, Stillbirth N, 2015 Clinical sensitivity and specificity of meconium fatty acid ethyl ester, ethyl glucuronide, and ethyl sulfate for detecting maternal drinking during pregnancy. Clin Chem 61, 523–532. [PubMed: 25595440]

Hlushchenko I, Koskinen M, Hotulainen P, 2016 Dendritic spine actin dynamics in neuronal maturation and synaptic plasticity. Cytoskeleton (Hoboken) 73, 435–441. [PubMed: 26849484]

Hoyme HE, Kalberg WO, Elliott AJ, Blankenship J, Buckley D, Marais AS, Manning MA, Robinson LK, Adam MP, Abdul-Rahman O, Jewett T, Coles CD, Chambers C, Jones KL, Adnams CM, Shah

PE, Riley EP, Charness ME, Warren KR, May PA, 2016 Updated Clinical Guidelines for Diagnosing Fetal Alcohol Spectrum Disorders. Pediatrics 138.

Hsieh S, Sapkota A, Wood R, Bearer C, Kapoor S, 2018 Neonatal ethanol exposure from ethanol-based hand sanitisers in isolettes. Arch Dis Child Fetal Neonatal Ed 103, F55–F58. [PubMed: 28588125]

Idrus NM, McGough NN, Riley EP, Thomas JD, 2014 Administration of memantine during withdrawal mitigates overactivity and spatial learning impairments associated with neonatal alcohol exposure in rats. Alcohol Clin Exp Res 38, 529–537. [PubMed: 24428701]

Ikonomidou C, Bittigau P, Ishimaru MJ, Wozniak DF, Koch C, Genz K, Price MT, Stefovska V, Horster F, Tenkova T, Dikranian K, Olney JW, 2000 Ethanol-induced apoptotic neurodegeneration and fetal alcohol syndrome. Science 287, 1056–1060. [PubMed: 10669420]

Ikonomidou C, Bosch F, Miksa M, Bittigau P, Vockler J, Dikranian K, Tenkova TI, Stefovska V, Turski L, Olney JW, 1999 Blockade of NMDA receptors and apoptotic neurodegeneration in the developing brain. Science 283, 70–74. [PubMed: 9872743]

Jiang Q, Hu Y, Wu P, Cheng X, Li M, Yu D, Deng J, 2007 Prenatal alcohol exposure and the neuroapoptosis with long-term effect in visual cortex of mice. Alcohol Alcohol 42, 285–290. [PubMed: 17537831]

Kalant H, 1993 Problems in the search for mechanisms of tolerance. Alcohol Alcohol Suppl 2, 1–8.

Kelly SJ, Lawrence CR, 2008 Intragastric intubation of alcohol during the perinatal period. Methods Mol Biol 447, 101–110. [PubMed: 18369914]

Kirischuk S, Sinning A, Blanquie O, Yang JW, Luhmann HJ, Kilb W, 2017 Modulation of Neocortical Development by Early Neuronal Activity: Physiology and Pathophysiology. Frontiers in cellular neuroscience 11, 379. [PubMed: 29238291]

Kirmse K, Kummer M, Kovalchuk Y, Witte OW, Garaschuk O, Holthoff K, 2015 GABA depolarizes immature neurons and inhibits network activity in the neonatal neocortex in vivo. Nat Commun 6, 7750. [PubMed: 26177896]

Kleiber ML, Laufer BI, Stringer RL, Singh SM, 2014 Third trimester-equivalent ethanol exposure is characterized by an acute cellular stress response and an ontogenetic disruption of genes critical for synaptic establishment and function in mice. Dev Neurosci 36, 499–519. [PubMed: 25278313]

Kostovic I, Jovanov-Milosevic N, 2006 The development of cerebral connections during the first 20–45 weeks' gestation. Semin Fetal Neonatal Med 11, 415–422. [PubMed: 16962836]

Lebedeva J, Zakharov A, Ogievetsky E, Minlebaeva A, Kurbanov R, Gerasimova E, Sitdikova G, Khazipov R, 2017 Inhibition of Cortical Activity and Apoptosis Caused by Ethanol in Neonatal Rats In Vivo. Cereb Cortex 27, 1068–1082. [PubMed: 26646511]

Lein ES, Hawrylycz MJ, Ao N, Ayres M, Bensinger A, Bernard A, Boe AF, Boguski MS, Brockway KS, Byrnes EJ, Chen L, Chen L, Chen TM, Chin MC, Chong J, Crook BE, Czaplinska A, Dang CN, Datta S, Dee NR, Desaki AL, Desta T, Diep E, Dolbeare TA, Donelan MJ, Dong HW, Dougherty JG, Duncan BJ, Ebbert AJ, Eichele G, Estin LK, Faber C, Facer BA, Fields R, Fischer SR, Fliss TP, Frensley C, Gates SN, Glattfelder KJ, Halverson KR, Hart MR, Hohmann JG, Howell MP, Jeung DP, Johnson RA, Karr PT, Kawal R, Kidney JM, Knapik RH, Kuan CL, Lake JH, Laramee AR, Larsen KD, Lau C, Lemon TA, Liang AJ, Liu Y, Luong LT, Michaels J, Morgan JJ, Morgan RJ, Mortrud MT, Mosqueda NF, Ng LL, Ng R, Orta GJ, Overly CC, Pak TH, Parry SE, Pathak SD, Pearson OC, Puchalski RB, Riley ZL, Rockett HR, Rowland SA, Royall JJ, Ruiz MJ, Sarno NR, Schaffnit K, Shapovalova NV, Sivisay T, Slaughterbeck CR, Smith SC, Smith KA, Smith BI, Sodt AJ, Stewart NN, Stumpf KR, Sunkin SM, Sutram M, Tam A, Teemer CD, Thaller C, Thompson CL, Varnam LR, Visel A, Whitlock RM, Wohnoutka PE, Wolkey CK, Wong VY, Wood M, Yaylaoglu MB, Young RC, Youngstrom BL, Yuan XF, Zhang B, Zwingman TA, Jones AR, 2007 Genome-wide atlas of gene expression in the adult mouse brain. Nature 445, 168–176. [PubMed: 17151600]

Lewin M, Ilina M, Betz J, Masiello K, Hui M, Wilson DA, Saito M, 2018 Developmental Ethanol-Induced Sleep Fragmentation, Behavioral Hyperactivity, Cognitive Impairment and Parvalbumin Cell Loss are Prevented by Lithium Co-treatment. Neuroscience 369, 269–277. [PubMed: 29183826]

Lewis B, Wellmann KA, Barron S, 2007 Agmatine reduces balance deficits in a rat model of third trimester binge-like ethanol exposure. Pharmacol Biochem Behav 88, 114–121. [PubMed: 17714770]

Lewis B, Wellmann KA, Kehrberg AM, Carter ML, Baldwin T, Cohen M, Barron S, 2012 Behavioral deficits and cellular damage following developmental ethanol exposure in rats are attenuated by CP-101,606, an NMDAR antagonist with unique NR2B specificity. Pharmacol Biochem Behav 100, 545–553. [PubMed: 22037411]

Leys C, Schumann S, 2010 A nonparametric method to analyze interactions: The adjusted rank transform test. Journal of Experimental Social Psychology 46, 684–688.

Li H, Wen W, Xu H, Wu H, Xu M, Frank JA, Luo J, 2019 4-Phenylbutyric Acid Protects Against Ethanol-Induced Damage in the Developing Mouse Brain. Alcohol Clin Exp Res 43, 69–78. [PubMed: 30403409]

Li HF, Mochly-Rosen D, Kendig JJ, 2005 Protein kinase Cgamma mediates ethanol withdrawal hyper-responsiveness of NMDA receptor currents in spinal cord motor neurons. Br J Pharmacol 144, 301–307. [PubMed: 15655532]

Lotfullina N, Khazipov R, 2018 Ethanol and the Developing Brain: Inhibition of Neuronal Activity and Neuroapoptosis. Neuroscientist 24, 130–141. [PubMed: 28580823]

Lovinger DM, White G, Weight FF, 1990 NMDA receptor-mediated synaptic excitation selectively inhibited by ethanol in hippocampal slice from adult rat. J Neurosci 10, 1372–1379. [PubMed: 2158533]

Lu C, Fu W, Mattson MP, 2001 Caspase-mediated suppression of glutamate (AMPA) receptor channel activity in hippocampal neurons in response to DNA damage promotes apoptosis and prevents necrosis: implications for neurological side effects of cancer therapy and neurodegenerative disorders. Neurobiol Dis 8, 194–206. [PubMed: 11300717]

Mameli M, Zamudio PA, Carta M, Valenzuela CF, 2005 Developmentally regulated actions of alcohol on hippocampal glutamatergic transmission. J Neurosci 25, 8027–8036. [PubMed: 16135760]

Mazzoni F, Muller C, DeAssis J, Lew D, Leevy WM, Finnemann SC, 2019 Non-invasive in vivo fluorescence imaging of apoptotic retinal photoreceptors. Sci Rep 9, 1590. [PubMed: 30733587]

Miller MW, 2006 Effect of prenatal exposure to ethanol on glutamate and GABA immunoreactivity in macaque somatosensory and motor cortices: critical timing of exposure. Neuroscience 138, 97–107. [PubMed: 16427209]

Mitchell AS, Czajkowski R, Zhang N, Jeffery K, Nelson AJD, 2018 Retrosplenial cortex and its role in spatial cognition. Brain Neurosci Adv 2, 2398212818757098.

Miyakawa T, Yagi T, Kitazawa H, Yasuda M, Kawai N, Tsuboi K, Niki H, 1997 Fyn-kinase as a determinant of ethanol sensitivity: relation to NMDA-receptor function [see comments]. Science 278, 698–701. [PubMed: 9381182]

Moore DB, Quintero MA, Ruygrok AC, Walker DW, Heaton MB, 1998 Prenatal ethanol exposure reduces parvalbumin-immunoreactive GABAergic neuronal number in the adult rat cingulate cortex. Neurosci Lett 249, 25–28. [PubMed: 9672380]

Moore DB, Ruygrok AC, Walker DW, Heaton MB, 1997 Effects of prenatal ethanol exposure on parvalbumin-expressing GABAergic neurons in the adult rat medial septum. Alcohol Clin Exp Res 21, 849–856. [PubMed: 9267534]

Morton RA, Diaz MR, Topper LA, Valenzuela CF, 2014 Construction of vapor chambers used to expose mice to alcohol during the equivalent of all three trimesters of human development. J. Vis. Exp 13 (89). doi: 10.3791/51839.

Moykkynen T, Korpi ER, 2012 Acute effects of ethanol on glutamate receptors. Basic Clin Pharmacol Toxicol 111, 4–13. [PubMed: 22429661]

Murphy DJ, Dunney C, Mullally A, Adnan N, Fahey T, Barry J, 2014 A prospective cohort study of alcohol exposure in early and late pregnancy within an urban population in Ireland. Int J Environ Res Public Health 11, 2049–2063. [PubMed: 24549147]

Niclasen J, Andersen AM, Strandberg-Larsen K, Teasdale TW, 2014 Is alcohol binge drinking in early and late pregnancy associated with behavioural and emotional development at age 7 years? Eur Child Adolesc Psychiatry 23, 1175–1180. [PubMed: 24390718]

Nikolic M, Gardner HA, Tucker KL, 2013 Postnatal neuronal apoptosis in the cerebral cortex: physiological and pathophysiological mechanisms. Neuroscience 254, 369–378. [PubMed: 24076086]

Olney JW, 2014 Focus on apoptosis to decipher how alcohol and many other drugs disrupt brain development. Frontiers in pediatrics 2, 81. [PubMed: 25136546]

Olney JW, Tenkova T, Dikranian K, Qin YQ, Labruyere J, Ikonomidou C, 2002 Ethanol-induced apoptotic neurodegeneration in the developing C57BL/6 mouse brain. Brain Res Dev Brain Res 133, 115–126. [PubMed: 11882342]

Paxinos G, Franklin KBJ, 2013 Paxinos and Franklin's The Mouse Brain in Stereotaxic Coordinates. Elsevier.

Petit-Paitel A, Menard B, Guyon A, Beringue V, Nahon JL, Zsurger N, Chabry J, 2012 Prion protein is a key determinant of alcohol sensitivity through the modulation of N-methyl-D-aspartate receptor (NMDAR) activity. PLoS One 7, e34691. [PubMed: 22536327]

Popova S, Lange S, Probst C, Gmel G, Rehm J, 2017 Estimation of national, regional, and global prevalence of alcohol use during pregnancy and fetal alcohol syndrome: a systematic review and meta-analysis. Lancet Glob Health 5, e290–e299. [PubMed: 28089487]

Preibisch S, Saalfeld S, Tomancak P, 2009 Globally optimal stitching of tiled 3D microscopic image acquisitions. Bioinformatics 25, 1463–1465. [PubMed: 19346324]

Puglia MP, Valenzuela CF, 2010 Ethanol acutely inhibits ionotropic glutamate receptor-mediated responses and long-term potentiation in the developing CA1 hippocampus. Alcohol Clin Exp Res 34, 594–606. [PubMed: 20102565]

Rachdaoui N, Li L, Willard B, Kasumov T, Previs S, Sarkar D, 2017 Turnover of histones and histone variants in postnatal rat brain: effects of alcohol exposure. Clin Epigenetics 9, 117. [PubMed: 29075360]

Ron D, Wang J, 2009 The NMDA Receptor and Alcohol Addiction. In: Van Dongen AM, (Ed), Biology of the NMDA Receptor, Boca Raton (FL).

Saito M, Chakraborty G, Hui M, Masiello K, Saito M, 2016 Ethanol-Induced Neurodegeneration and Glial Activation in the Developing Brain. Brain Sci 6.

Saito M, Mao RF, Wang R, Vadasz C, Saito M, 2007 Effects of gangliosides on ethanol-induced neurodegeneration in the developing mouse brain. Alcohol Clin Exp Res 31, 665–674. [PubMed: 17374046]

Saito M, Smiley JF, Hui M, Masiello K, Betz J, Ilina M, Saito M, Wilson DA, 2019 Neonatal Ethanol Disturbs the Normal Maturation of Parvalbumin Interneurons Surrounded by Subsets of Perineuronal Nets in the Cerebral Cortex: Partial Reversal by Lithium. Cereb Cortex 29, 1383–1397. [PubMed: 29462278]

Sanderson JL, Donald Partridge L, Valenzuela CF, 2009 Modulation of GABAergic and glutamatergic transmission by ethanol in the developing neocortex: an in vitro test of the excessive inhibition hypothesis of fetal alcohol spectrum disorder. Neuropharmacology 56, 541–555. [PubMed: 19027758]

Scheirer CJ, Ray WS, Hare N, 1976 The analysis of ranked data derived from completely randomized factorial designs. Biometrics 32, 429–434. [PubMed: 953139]

Schneider CA, Rasband WS, Eliceiri KW, 2012 NIH Image to ImageJ: 25 years of image analysis. Nature methods 9, 671–675. [PubMed: 22930834]

Skorput AG, Gupta VP, Yeh PW, Yeh HH, 2015 Persistent Interneuronopathy in the Prefrontal Cortex of Young Adult Offspring Exposed to Ethanol In Utero. J Neurosci 35, 10977–10988. [PubMed: 26245961]

Smiley JF, Saito M, Bleiwas C, Masiello K, Ardekani B, Guilfoyle DN, Gerum S, Wilson DA, Vadasz C, 2015 Selective reduction of cerebral cortex GABA neurons in a late gestation model of fetal alcohol spectrum disorder. Alcohol 49, 571–580. [PubMed: 26252988]

Subbanna S, Joshi V, Basavarajappa BS, 2018 Activity-dependent Signaling and Epigenetic Abnormalities in Mice Exposed to Postnatal Ethanol. Neuroscience 392, 230–240. [PubMed: 30031835]

Sugar J, Witter MP, van Strien NM, Cappaert NL, 2011 The retrosplenial cortex: intrinsic connectivity and connections with the (para)hippocampal region in the rat. An interactive connectome. Front Neuroinform 5, 7. [PubMed: 21847380]

Swartzwelder HS, Wilson WA, Tayyeb MI, 1995 Differential sensitivity of NMDA receptor-mediated synaptic potentials to ethanol in immature versus mature hippocampus. Alcohol Clin Exp Res 19, 320–323. [PubMed: 7625564]

Thomas JD, Fleming Sl, Riley EP, 2001 MK-801 can exacerbate or attenuate behavioral alterations associated with neonatal alcohol exposure in the rat, depending on the timing of administration. Alcohol Clin Exp Res 25, 764–773. [PubMed: 11371726]

Thomas JD, Garcia GG, Dominguez HD, Riley EP, 2004 Administration of eliprodil during ethanol withdrawal in the neonatal rat attenuates ethanol-induced learning deficits. Psychopharmacology (Berl) 175, 189–195. [PubMed: 15064913]

Toesca A, Giannetti S, Granato A, 2003 Overexpression of the p75 neurotrophin receptor in the sensori-motor cortex of rats exposed to ethanol during early postnatal life. Neurosci Lett 342, 89–92. [PubMed: 12727325]

Valeeva G, Tressard T, Mukhtarov M, Baude A, Khazipov R, 2016 An Optogenetic Approach for Investigation of Excitatory and Inhibitory Network GABA Actions in Mice Expressing Channelrhodopsin-2 in GABAergic Neurons. J Neurosci 36, 5961–5973. [PubMed: 27251618]

Wang Y, Kakizaki T, Sakagami H, Saito K, Ebihara S, Kato M, Hirabayashi M, Saito Y, Furuya N, Yanagawa Y, 2009 Fluorescent labeling of both GABAergic and glycinergic neurons in vesicular GABA transporter (VGAT)-venus transgenic mouse. Neuroscience 164, 1031–1043. [PubMed: 19766173]

Wu PH, Coultrap SJ, Browning MD, Proctor WR, 2011 Functional adaptation of the N-methyl-D-aspartate receptor to inhibition by ethanol is modulated by striatal-enriched protein tyrosine phosphatase and p38 mitogen-activated protein kinase. Mol Pharmacol 80, 529–537. [PubMed: 21680777]

Yaka R, Phamluong K, Ron D, 2003 Scaffolding of Fyn kinase to the NMDA receptor determines brain region sensitivity to ethanol. J Neurosci 23, 3623–3632. [PubMed: 12736333]

You C, Savarese A, Vandegrift BJ, He D, Pandey SC, Lasek AW, Brodie MS, 2019 Ethanol acts on KCNK13 potassium channels in the ventral tegmental area to increase firing rate and modulate binge-like drinking. Neuropharmacology 144, 29–36. [PubMed: 30332606]

Ziburkus J, Dilger EK, Lo FS, Guido W, 2009 LTD and LTP at the developing retinogeniculate synapse. J Neurophysiol 102, 3082–3090. [PubMed: 19776360]

- Postnatal day 7 Venus-VGAT mice were exposed to vaporized ethanol for 4 h
- This triggered apoptotic neurodegeneration in the P7 mouse retrosplenial cortex
- Inhibition of firing evoked by synaptic input could contribute to this effect
- This effect is mediated, at least in part, by NMDA receptor inhibition
- There were differences in ethanol's effect in pyramidal neurons vs interneurons

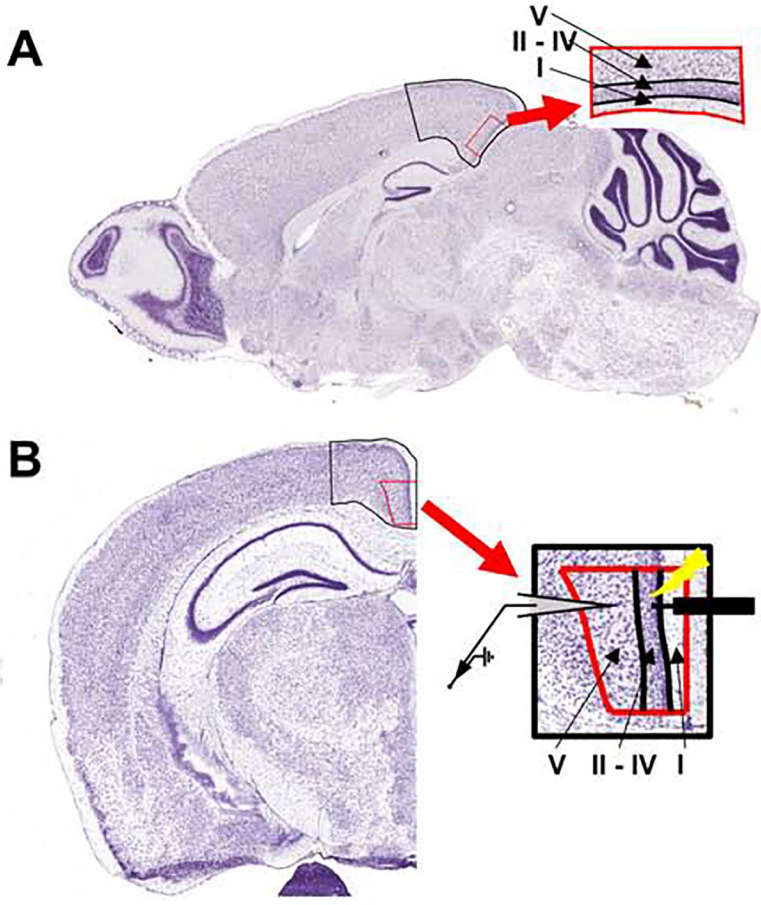

Figure 1. Atlas images outlining the location of the mouse retrosplenial cortex.

A) Representative parasagittal tissue section from an adult mouse with the retrosplenial cortex outlined in black. The enlarged red-outlined inset shows the different cortical layers. All immunohistochemistry experiments were performed using equivalent parasagittal tissue sections from mouse pups. B) Coronal tissue section from an adult mouse with the retrosplenial cortex outlined in black. The enlarged red-outlined inset shows the different cortical layers, as well as the placement of concentric bipolar stimulating (right) and recording (left) electrodes used for electrophysiology experiments in slices from mouse pups. Images adapted from the Allen Developing Mouse Brain Atlas (https://mouse.brain-map.org/static/atlas) (Lein et al., 2007). Image credit: Allen Institute.

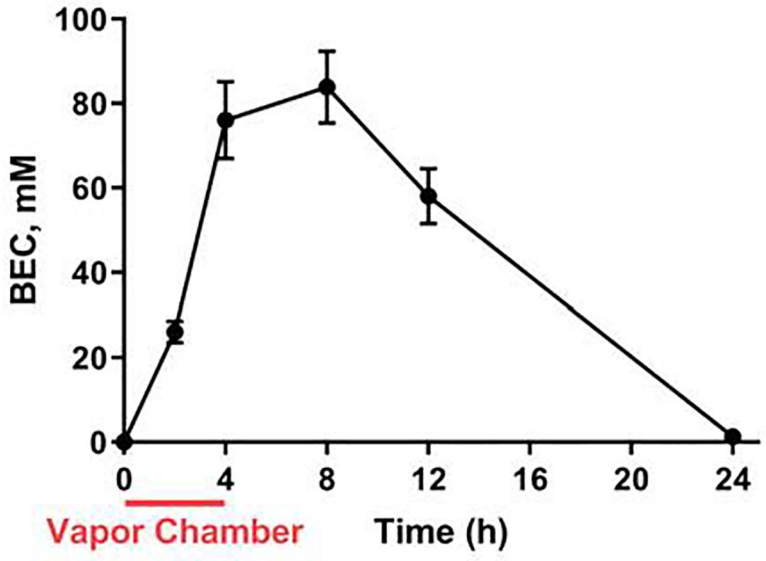

Figure 2. Blood ethanol concentrations (BECs) following vapor chamber exposure.

BEC (n = 4 animals from 2–4 litters per time point) evaluated at the indicated time points. The interval when vapor chamber exposure took place is indicated by the red line. See Supplementary Table 1 for results of statistical analyses.

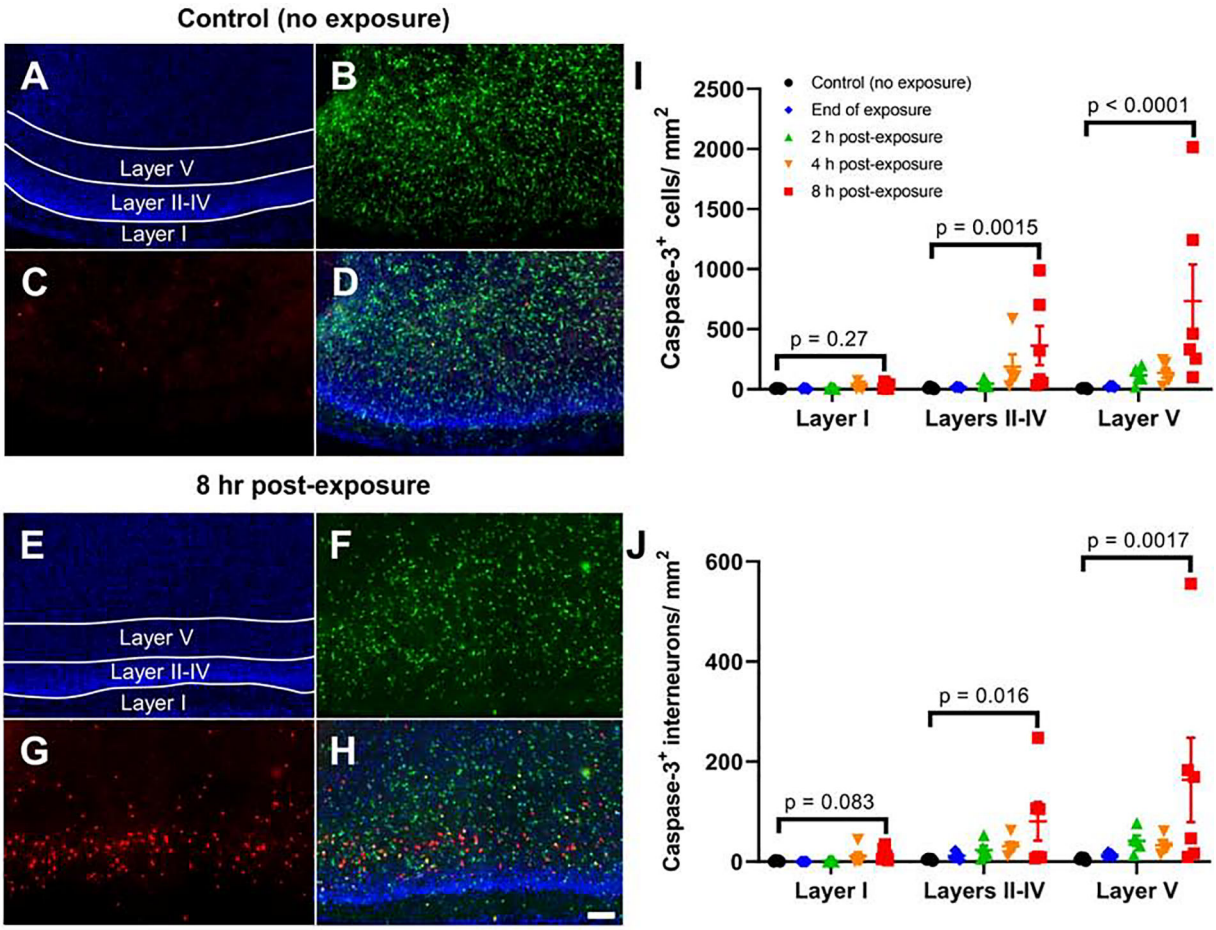

Figure 3. Exposure to ethanol at P7 increases cleaved caspase-3 levels in the mouse RSC.

Shown are representative images of RSC tissue sections stained for cleaved caspase-3 from a non-exposed control mouse (A-D) and a mouse euthanized 8 h post-vapor chamber exposure (E-H) (10X objective, scale bar = 100 μm). Panels A&E show DAPI-stained nuclei, panels B&F show Venus-positive interneurons, panels C&G show cleaved-caspase-3 IHC, and panels D&H show the merged images. I) The total number of cleaved caspase-3 positive cells per mm^2 in the RSC are shown for control brains and brains collected at different intervals following vapor chamber exposure (end of exposure, 2, 4, and 8 h post-exposure). J) The total numbers of cleaved caspase-3 positive interneurons (positive for both cleaved caspase-3 and Venus) per mm^2 are shown. Bonferroni corrected p-values presented in each graph show the result of a Dunn's multiple comparison post-hoc test comparing the control and 8-h time points within layer. Results of two-way non-parametric tests, as well as pairwise comparisons between control and other time points within layer, are presented in Supplemental Table 1. n = 5–6 animals from 5 litters per time point. Data presented are individual values with mean ± SEM.

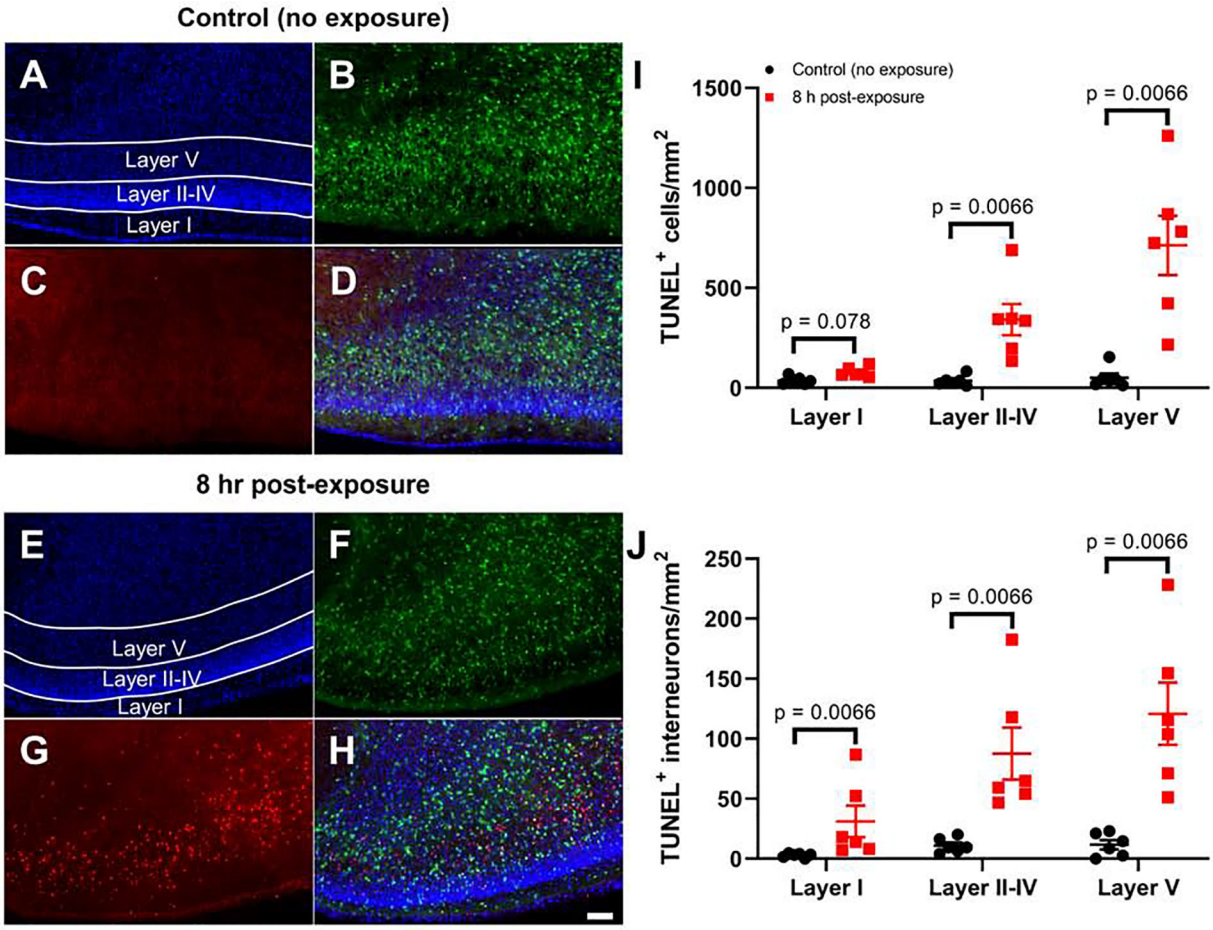

Figure 4. Exposure to ethanol at P7 causes apoptotic DNA damage in cells from the mouse RSC as measured by TUNEL staining.

Shown are representative images of the RSC from a non-exposed control mouse (A-D) and a mouse euthanized 8 h post-vapor chamber exposure (E-H) (10X objective, scale bar = 100 μm). Panels A&E show DAPI-stained nuclei, panels B&F show Venus-positive interneurons, panels C&G show TUNEL positive cells, and panels D&H show the merged images. I) The total numbers of TUNEL positive cells per mm^2 in the RSC are shown for control brains and brains collected 8 h after the vapor chamber exposure. J) The total numbers of TUNEL positive interneurons (positive for both TUNEL and Venus) per mm^2 are shown. Bonferroni corrected p-values presented in each graph show the result of Mann-Whitney U post-hoc tests comparing the control and 8-h time points within layer. Results of two-way non-parametric tests are presented in Supplemental Table 1. n = 6 animals from 6 litters per time point. Data presented are individual values with mean ± SEM.

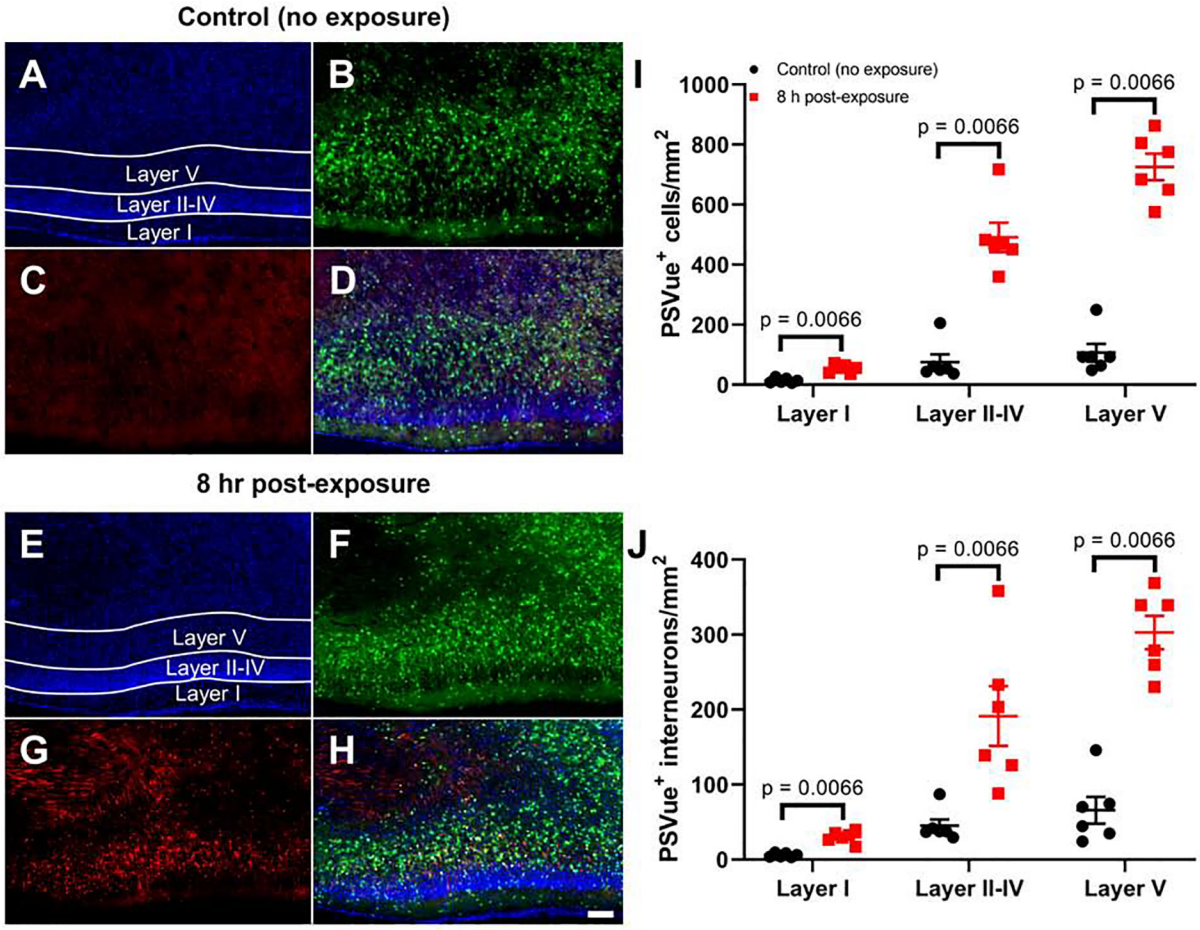

Figure 5. Exposure to ethanol at P7 leads to an increase in externally exposed anionic phospholipids, a hallmark of apoptosis, as measured by PSVue 550 staining.

Shown are representative images of the RSC from a non-exposed control mouse (A-D) and a mouse euthanized 8 h post-vapor chamber exposure (E-H) (10X objective, scale bar = 100 μm). Panels A&E show DAPI nuclei, panels B&F show Venus-positive interneurons, panels C&G show PSVue positive cells, and panels D&H show the merged images. I) The total numbers of PSVue positive cells per mm^2 in the RSC are shown for control brains and brains collected 8 h after the vapor chamber exposure. J) The total numbers of PSVue positive interneurons (positive for both PSVue and Venus) per mm^2 are shown. Bonferroni corrected p-values presented in each graph show the result of Mann-Whitney U post-hoc tests comparing the control and 8-h time points within layer. Results of two-way non-parametric tests are presented in Supplemental Table 1. n = 6 animals from 6 litters per time point. Data presented are individual values with mean ± SEM.

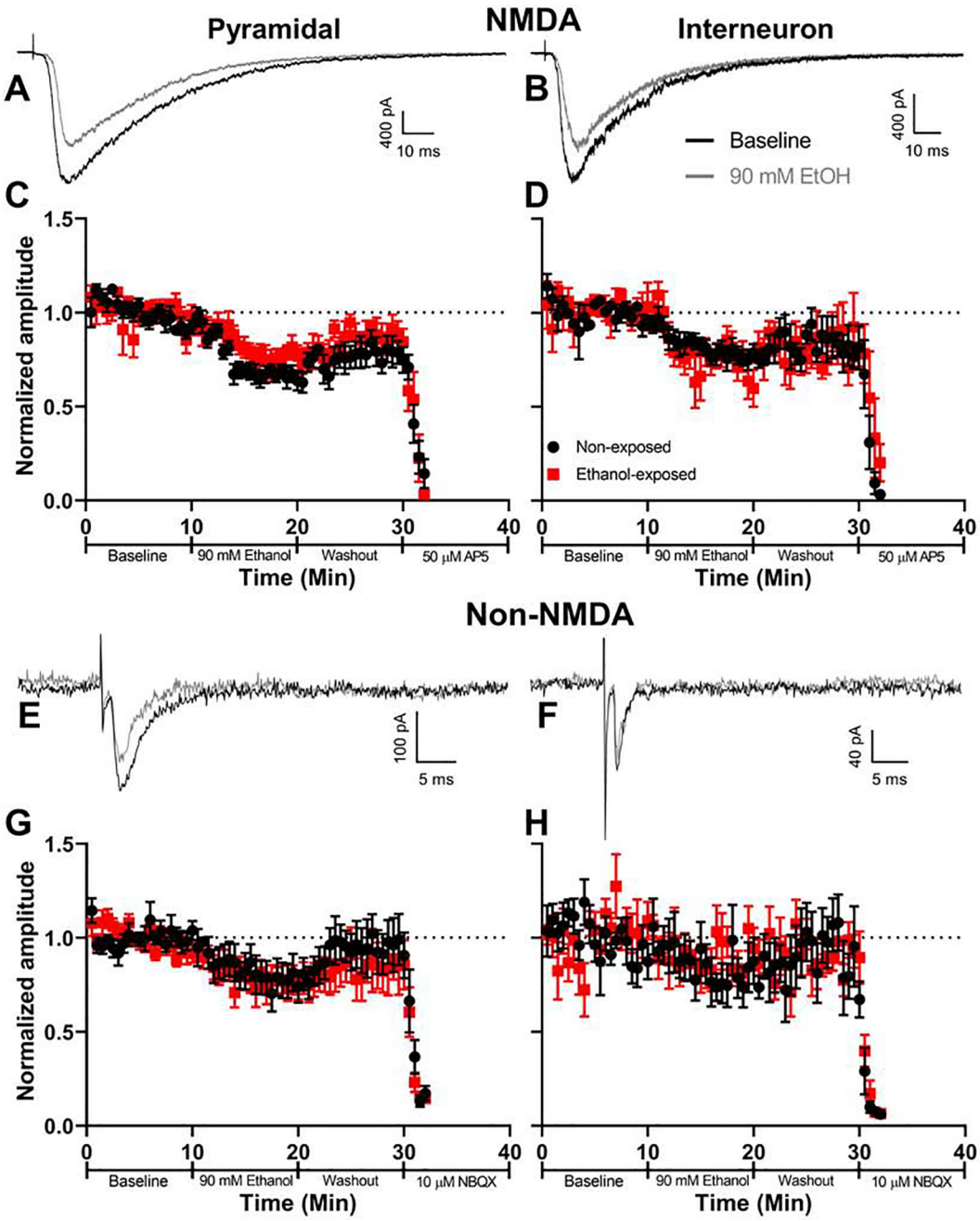

Figure 6. Acute bath application of ethanol decreases evoked NMDA and non-NMDA current amplitude in both pyramidal neurons and interneurons, and these cells do not develop tolerance to this effect after *in vivo* vapor chamber exposure.

Representative evoked NMDA EPSC traces are shown for (A) pyramidal neurons and (B) interneurons during baseline (black traces) and acute 90 mM ethanol bath application (grey traces) in animals not exposed to vaporized ethanol *in vivo.* Normalized NMDA EPSC amplitudes from (C) pyramidal neurons (non-exposed n = 9 animals (1 cell per animal, each from a different litter), ethanol-exposed n = 8 animals (1 cell per animal, each from a different litter)) and (D) interneurons (non-exposed and ethanol-exposed n = 7 animals (1 cell per animal, each from a different litter)) in brain slices taken from animals before (black

circles) or after 4-h vapor chamber exposure (red squares). Representative evoked non-NMDA EPSC traces are shown for (E) pyramidal neurons and (F) interneurons recorded during baseline and acute 90 mM ethanol bath application. Detailed examination of paired-pulse ratios is shown in Supplemental Fig 2. Normalized non-NMDA amplitudes from (G) pyramidal neurons (non-exposed and ethanol-exposed n = 8 animals (1 cell per animal, each from a different litter)) and (H) interneurons (non-exposed n = 6 animals (7 cells from 6 litters), ethanol-exposed n = 7 animals (1 cell per animal, each from a different litter)) taken from animals before or after vapor chamber exposure. Data points are mean ± SEM.

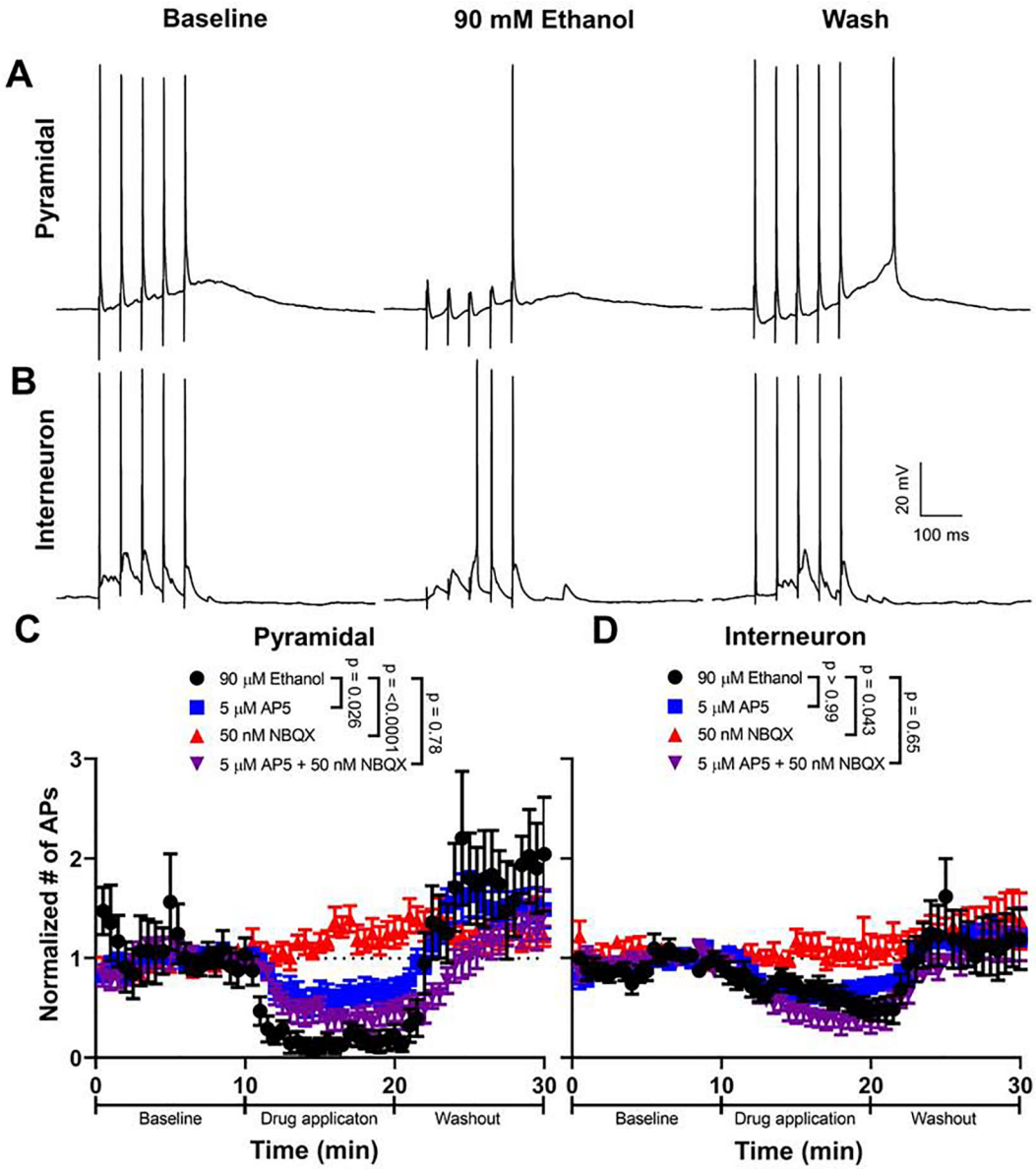

Figure 7. Acute bath application of ethanol reduces synaptically-induced action potential firing in both pyramidal neurons and interneurons.

Representative traces of current-clamp recordings from A) pyramidal neurons and B) interneurons obtained at baseline, during 90 mM ethanol bath application, and washout. Mice were not exposed to ethanol in vapor chambers for these experiments. Normalized action potential numbers are shown for C) pyramidal neurons and D) interneurons during application and washout of either 90 mM ethanol (pyramidal n = 11 cells (from 9 animals from 7 litters); interneuron n = 11 cells (from 10 animals from 6 litters)), 5 μM DL-AP5 (pyramidal n = 10 cells (from 10 animals from 7 litters); interneuron n = 11 cells (from 11 animals from 8 litters)), 50 nM NBQX (pyramidal n = 11 cells (from 11 animals from 8 litters); interneuron n = 10 cells (from 10 animals from 8 litters)), or 5 μM-AP5 + 50 nM NBQX (pyramidal n = 13 cells (from 10 animals from 6 litters); interneuron n = 11 cells (from 10 animals from 6 litters)). Action potential firing analyses were carried out in

animals that were not exposed to ethanol *in vivo* via vapor chambers. Bonferroni corrected p-values presented show the result of a parametric or non-parametric multiple comparison test comparing how the different drugs changed action potential number compared to 90 mM ethanol. For a detailed presentation of statistical analyses, please see Supplemental Table 1. Data points are mean ± SEM for the normalized number of action potentials.

Table 1.

Characteristics of glutamatergic excitatory postsynaptic currents (EPSCs) in pyramidal neurons and interneurons from control and ethanol vapor-exposed animals.

A) Characteristics of NMDA EPSCs. B) Characteristics of non-NMDA EPSCs. Data presented are mean(SEM) values. Sample sizes given indicate number of animals used (1 cell per animal, each from a single litter). For a detailed presentation of parametric and non-parametric tests performed comparing exposure condition within cell type please see Supplemental Table 1.

A	NMDA			
	Pyramidal		Interneuron	
	No Exposure	Ethanol Exposed	No Exposure	Ethanol Exposed
	(n = 9)	(n = 8)	(n = 7)	(n = 7)
Rise time (ms)	61.17(9.10)	62.85(6.73)	55.66(7.83)	48.02(5.25)
Decay tau (ms)	435.18(33.59)	387.57(25.67)	375.19(94.74)	290.75(35.03)
Peak current (pA)	4088.80(458.97)	4827.47(926.38)	2090.55(350.37)	2850.81(416.6)
Current density (pA/pF)	33.48(2.02)	39.73(7.17)	42.10(4.77)	51.65(7.71)
Membrane resistance (MΩ)	121.55(15.79)	157.10(32.36)	505.12(221.59)	269.29(65.83)
Membrane capacitance (pF)	121.41(9.96)	119.70(9.62)	50.16(7.59)	55.55(5.41)
B	Non-NMDA			
	Pyramidal		Interneuron	
	No Exposure	Ethanol Exposed	No Exposure	Ethanol Exposed
	(n = 8)	(n = 8)	(n = 6)	(n = 7)
Rise time (ms)	1.18(0.25)	1.2(0.24)	0.73(0.08)	0.64(0.06)
Decay tau (ms)	3.93(0.86)	3.82(0.6)	1.73(0.16)	1.76(0.12)
Peak current (pA)	234.35(46.72)	196.01(36.03)	306.39(98.24)	482.41(90.01)
Current density (pA/pF)	2.44(0.47)	2.16(0.43)	5.99(1.8)	9.3(2.23)
Paired pulse ratio (P2/P1)	1.17(0.15)	1.28(0.12)	0.93(0.18)	1.41(0.29)
Membrane resistance (MΩ)	184.44(59.1)	168.58(30.28)	207.38(45.07)	230.06(54.2)
Membrane capacitance (pF)	102.59(11.63)	94.84(7.11)	51.96(4.1)	59.78(6.76)